Precambrian Research 254 (2014) 210–225

Contents lists available at ScienceDirect

Precambrian Research

journal homepage: www.elsevier.com/locate/precamres

The Paleoproterozoic magmatic–metamorphic events and cover sediments of the Tiekelik Belt and their tectonic implications for the southern margin of the Tarim Craton, northwestern China

Chao Wang[a,*], Yong-He Wang[a], Liang Liu[b], Shi-Ping He[a], Rong-She Li[a], Meng Li[a], Wen-Qiang Yang[b], Yu-Ting Cao[c], Joseph G. Meert[d], Chao Shi[a]

[a] MLR Key Laboratory of Genesis and Exploration of Magmatic Ore Deposits, Orogen Research Centre of China Geological Survey, Xi'an Center of Geological Survey, Xi'an 710054, China
[b] State Key Laboratory of Continental Dynamics, Department of Geology, Northwest University, Xi'an 710069, China
[c] College of Geological Science & Engineering, Shandong University of Science and Technology, Qingdao 266510, China
[d] Department of Geological Sciences, University of Florida, 241 Williamson Hall, Gainesville, FL 32611, USA

ARTICLE INFO

Article history:
Received 28 April 2014
Received in revised form 25 August 2014
Accepted 27 August 2014
Available online 16 September 2014

Keywords:
Zircon U–Pb dating
Tarim craton
A-type granite
Paleoproterozoic
Columbia

ABSTRACT

The Tiekelik Belt in the southwestern part of the Tarim Craton, NW China, consists of Archean–Paleoproterozoic orthogneisses, and granitoids, and younger sedimentary successions. U–Pb dating of Paleoproterozoic rocks in the Tiekelik Belt has provided new information on the southwestern margin of the Tarim Craton. Two orthogneisses from the Heluositan Complex yielded crystallization ages in the interval 2310–2260 Ma and metamorphic ages of 2040–2007 Ma and 1830 Ma, respectively. Two syenogranites from the Buweituwei pluton yielded crystallization ages of 1900 and 1795 Ma. Detrital zircon analyses from sedimentary rocks nonconformably overlying the Buweituwei and Akazi plutons indicate maximum depositional ages between 1950 Ma and 1780 Ma. Major detrital inputs are from the basement in the region and form prominent peaks at 1900–1800 Ma and 2300–2200 Ma. Our new data, combined with previous results, allow us to summarize the Archean–Paleoproterozoic tectonic evolution of the Tiekelik Belt as follows: (1) Emplacement of Archean-aged TTG magmas during the 3.14–2.76 Ga interval; (2) A series of 2.41–2.26 Ga magmatic events that represent an important period of crustal reworking within the Tarim craton; (3) 2.03–1.80 Ga magmatic and metamorphic events that include the emplacement of a 1.9 Ga mafic dyke suite into the Heluositan Complex along with several episodes of intraplate magmatism. The late magmatic events are coeval with metamorphism and may support an orogenic extensional model for the Tiekelik Belt during the 1.9–1.8 Ga interval; (4) post-1.8 Ga subsidence and formation of a Changcheng sequence in the Tiekelik Belt. The Paleoproterozoic ages of major tectonothermal events within the Tiekelik, North Altyn–Dunhuang block and Alashan block are almost identical and it is argued that they were connected at that time as North China and Tarim were part of the larger Columbia supercontinent.

1. Introduction

There is now broad consensus that the global distribution of continental collisions documented between 2.1 and 1.8 Ga record the amalgamation of supercontinent Columbia (aka Nuna; Rogers and Santosh, 2002; Zhao et al., 2002, 2004; Meert, 2002, 2012). In some configurations of Columbia, the Tarim Craton was not included (Rogers and Santosh, 2002; Meert, 2002; Hou et al., 2008; Zhang et al., 2012a). Recent data suggest that the Tarim Craton was part of Columbia although its exact position within that continent is somewhat variable (Zhang et al., 2007, 2012b,c, 2013a,b; Shu et al., 2011; Long et al., 2012; Ma et al., 2013; Ge et al., 2013; He et al., 2013; Meert, 2014). As an example, in some models the Tarim Craton (TC) and the North China Craton (NCC) were separated (Zhao et al., 2002, 2004; Yakubchuk, 2010) whereas in others they remained connected (Rogers and Santosh, 2009; Ge et al., 2013; Zhang et al., 2012c, 2013b).

Situated in northwest China, the Tarim Craton is bounded by the Tianshan, Western Kunlun and Central–Southern Altyn Tagh mountain belts to the north, south and southeast, respectively

* Corresponding author. Tel.: +86 29 87821743; fax: +86 29 88304789.
E-mail addresses: wangc-mail@163.com, xawangchao@gmail.com (C. Wang).

http://dx.doi.org/10.1016/j.precamres.2014.08.018
0301-9268/

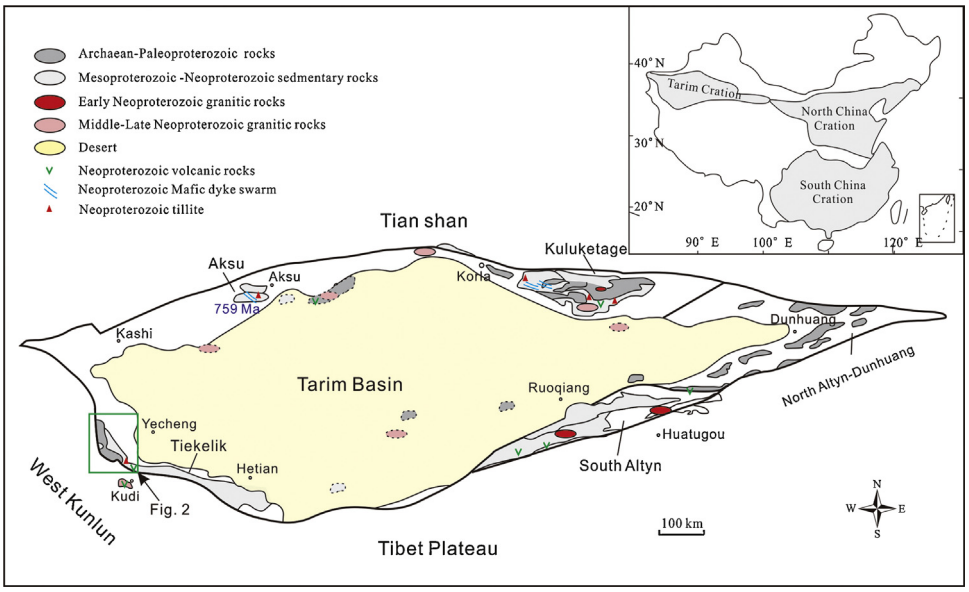

Fig. 1. Map of the Precambrian basement of the Tarim Craton. The dashed circles show the distribution of Precambrian rocks inferred from drill hole data. Inset shows location of the Tarim Craton within China.

(Fig. 1; Zhao and Cawood, 2012). Due to the extensive younger cover of the Taklamakan desert in the central part of the craton, the basement of the Tarim Craton is only exposed along the margins of the main basin (Fig. 1). These exposures include two regions along the southern margin of Tarim (Tiekelik and North Altyn–Dunhuang) and the Aksu and Kuluketage areas at the northern margin. The Archean–Paleoproterozoic aged basement rocks of the Tarim Craton are mainly exposed in the Kuruketage, North Altyn–Dunhuang and Tiekelik areas (Fig. 1; Gao and Zhu, 1984; Hu and Rogers, 1992; Lu and Yuan, 2003; Guo et al., 2003, 2013; Zhang et al., 2007, 2012b,c, 2013b; Lu et al., 2008; Long et al., 2010, 2012; Wang, 2011; Zong et al., 2013). Previously published data indicate that two major Paleoproterozoic 'events' took place at 2.45–2.25 Ga (magmatism) and 2.0–1.8 Ga (magmatism and metamorphism; Lu et al., 2008; Wang et al., 2009; Long et al., 2010; Shu et al., 2011; Wang, 2011; Zhang et al., 2012b,c,d, 2013b; Ge et al., 2013; He et al., 2013). Recently, new geochronological data were obtained from a deep drillhole into the basement of the Tarim craton. These data indicate that magmatic activity may have continued intermittently until c. 1.7 Ga and consisted of major reworking of the older Paleoproterozoic and Archean crust (Wu et al., 2012; Xu et al., 2013; Han et al., 2014).

The Tiekelik Belt is a narrow, but important, NW–SE-trending region along the southwestern margin of the Tarim Craton (Fig. 1). Rocks exposed in the Tiekelik Belt mainly consist of Paleoproterozoic and Neoproterozoic greenschist to amphibolite facies gneisses, schists, migmatites, amphibolites, quartzites, volcanic rocks and conglomerates that are overlain by late Palaeozoic to Cenozoic terrigenous sedimentary rocks (e.g. RGXR, 1993). The oldest rocks in the region are represented by a c. 3.14 Ga granitic gneiss (Guo et al., 2013). Zhang et al. (2007) argued that two Paleoproterozoic phases of high-K intrusions were emplaced at 2.41 and 2.34 Ga and were metamorphosed at 1.9 Ga. However, the sparse geochronological data do not fully constrain the Archean to Paleoproterozoic development of the Tiekelik Belt. In this paper, we present new zircon U–Pb geochronological data and whole rock geochemistry from different rock units within the region in order to unravel the architecture and evolution of the Tiekelik Belt during the Paleoproterozoic. Furthermore, a comparison of tectonothermal events from the Tiekelik and North Altyn–Dunhuang block and Alashan block are presented to evaluate the relationship between the Tarim Craton and North China Craton in the Columbia supercontinent.

2. Geological setting

The Tiekelik Belt is located in the southwestern part of the Tarim Craton between the Taklamakan desert and the West Kunlun Mountains (Fig. 1). The geological evolution of the Tiekelik Belt began with Archean to Paleoproterozoic thermo-magmatic episodes (of uncertain age) followed by the emplacement of c. 1.4 Ga anorogenic granitoids (Xu and Zhang, 1996; Zhang et al., 2007; Wang et al., 2009; Guo et al., 2013; Huang et al., 2012). The Archean and Paleoproterozoic geologic units within the belt (Fig. 2) are traditionally divided into (1) the Heluositan Group; (2) the Buweituwei and Akazi plutons; and (3) the Changcheng sedimentary sequence (1.8–1.6 Ga). The overlying Mesoproterozoic and Neoproterozoic sequences include continental rift volcanosedimentary deposits (Ma et al., 1991; Wang et al., 2004, 2009, 2014). A detailed discussion of the Neoproterozoic evolution of the Tiekelik Belt can be found in Wang et al. (2014 and references therein).

The Heluositan Group outcrops in the western part of the Tiekelek Belt and consists of paragneisses, orthogneisses and migmatites (Figs. 2 and 3a), most of which have been metamorphosed under upper amphibolite- to granulite-facies conditions (RGXR, 1993; Guo et al., 2013). Since it is composed of magmatic and high-grade metamorphic rocks, it is not a group in the stratigraphic sense, and we will refer to it as the Heluositan Complex. It is intruded by the c. 2.34 Ga Buweiduwei and c. 2.41 Ga Akazi granitoids (Xu and Zhang, 1996; Zhang et al., 2007) and 1.8 Ga mafic dykes (unpublished data; Fig. 3b). Recently, a protolith age of 3.14 Ga was obtained on a sample of granitic gneiss within the Heluositan Complex (Guo et al., 2013). Collectively, the available geochronology suggests that the protoliths of the Heluositan Complex formed in the Archean and early Paleoproterozoic; however, no metamorphic ages from the Heluositan Complex have yet been published.

The Buweituwei and Akazi plutons intrude the Heluositan Complex gneissic suite. The Buweituwei pluton (BP) is a polyphase pluton composed of gneissic granodiorite, monzogranite and syenogranite along with minor amphibolite (Fig. 4a; HNGS, 2004).

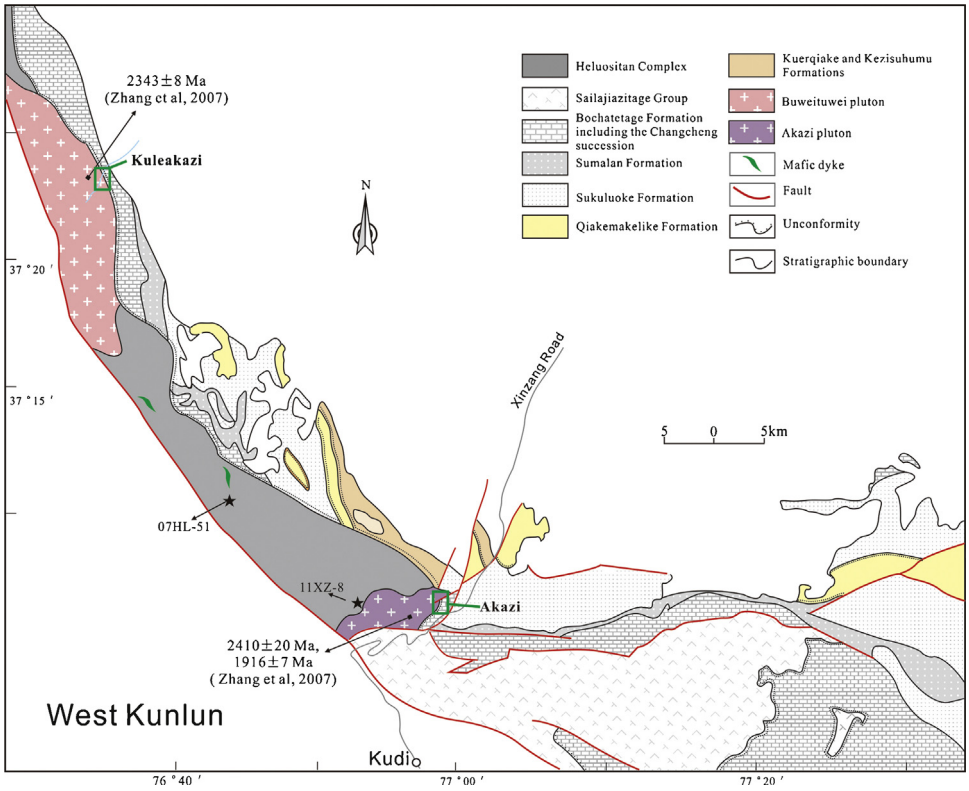

Fig. 2. Simplified regional geological map showing the Precambrian units in the western part of the Tiekelik Belt in SW Tarim with the locations of geochronological samples collected in this study (modified after HNGS, 2004). Study areas marked 'Akazi' and 'Kuleakazi' outlined by rectangles. Samples that are not marked individually on this map are from these two rectangles.

Zhang et al. (2004) argued that the amphibolites are the remnants of mafic rocks formed in an intraplate rift setting. The BP potassic granite suite from the Xuxugou area yielded a U–Pb crystallization age of 2343 ± 8 Ma (Zhang et al., 2007). This suite was further sub-divided into two subunits that were classified as A-type and S-type granites (Zhang et al., 2007). Both of the subunits have comparable Nd isotope compositions ($\varepsilon Nd(t) \approx -2.1$ to -0.4) and narrow Nd model ages ranges (2.91–2.76 Ga; Zhang et al., 2007). The Akazi pluton (AP) includes syenogranite and monzogranite bodies (HNGS, 2004). The two varieties are pink in color, medium to coarse grained and exhibit both gneissic and granitic textures. Both plutons are intruded by diabase dykes (Fig. 5a). Ages from the AP are constrained by two different studies. Zhang et al. (2007) obtained a 2410 ± 20 Ma (U–Pb, SHRIMP) crystallization age and a 1916 ± 7 Ma age that was interpreted as the timing of metamorphism. Xu and Zhang (1996) obtained a less precise upper intercept age of 2261 ± 95/75 Ma (TIMS). Zhang et al. (2007) interpreted the 2410 Ma granite as a late to post-orogenic A-type granite. $\varepsilon Nd(t)$ values for the suite range from −4.7 to −3.2 and the Nd model ages vary between 3.17 Ga and 3.05 Ga.

Both the AP and the BP intrusions are nonconformably overlain by younger sedimentary successions, known as the Changcheng sequences (Figs. 4 and 5). In the Kuleakazi area, the sedimentary sequences overlying the BP are (from lower to upper) known as the Klaker, Layileke and Bukatuwei formations (Ma et al., 1991). The Klaker Formation consists of coarse-grained sandstones, limestones and minor interbedded mudstones (Fig. 4d and e). The overlying Layilke and Bukatuwei Formations are comprised of feldspathic sandstones, limestones, dolomite and basalt (Fig. 4e; Ma et al., 1991; Wang et al., 2004).

There is considerable controversy regarding the ages of these overlying sedimentary sequences. Peng and Gao (1988) suggested that they are part of the Changcheng (1.8–1.6 Ga) sedimentary sequence based on a paleobotanical analysis. In contrast, the RGXR (1993) classified these rocks as part of the younger Jixian System (1.6–1.4 Ga) and referred to the sedimentary rocks as the

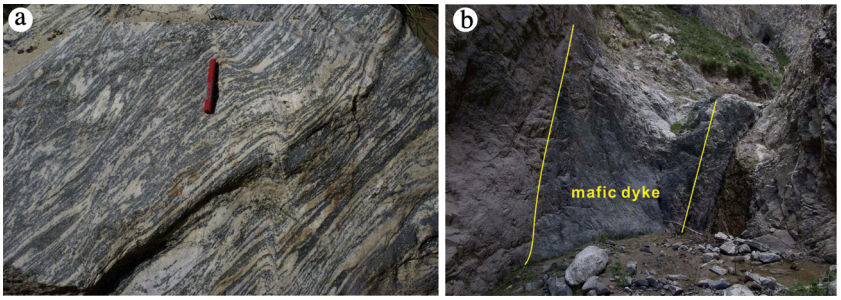

Fig. 3. Selected field photographs presenting the Heluositan Complex: (a) the deformation of orthogneisses investigated in this study; (b) Mafic dyke intruded into the orthogneisses of the Heluositan Complex.

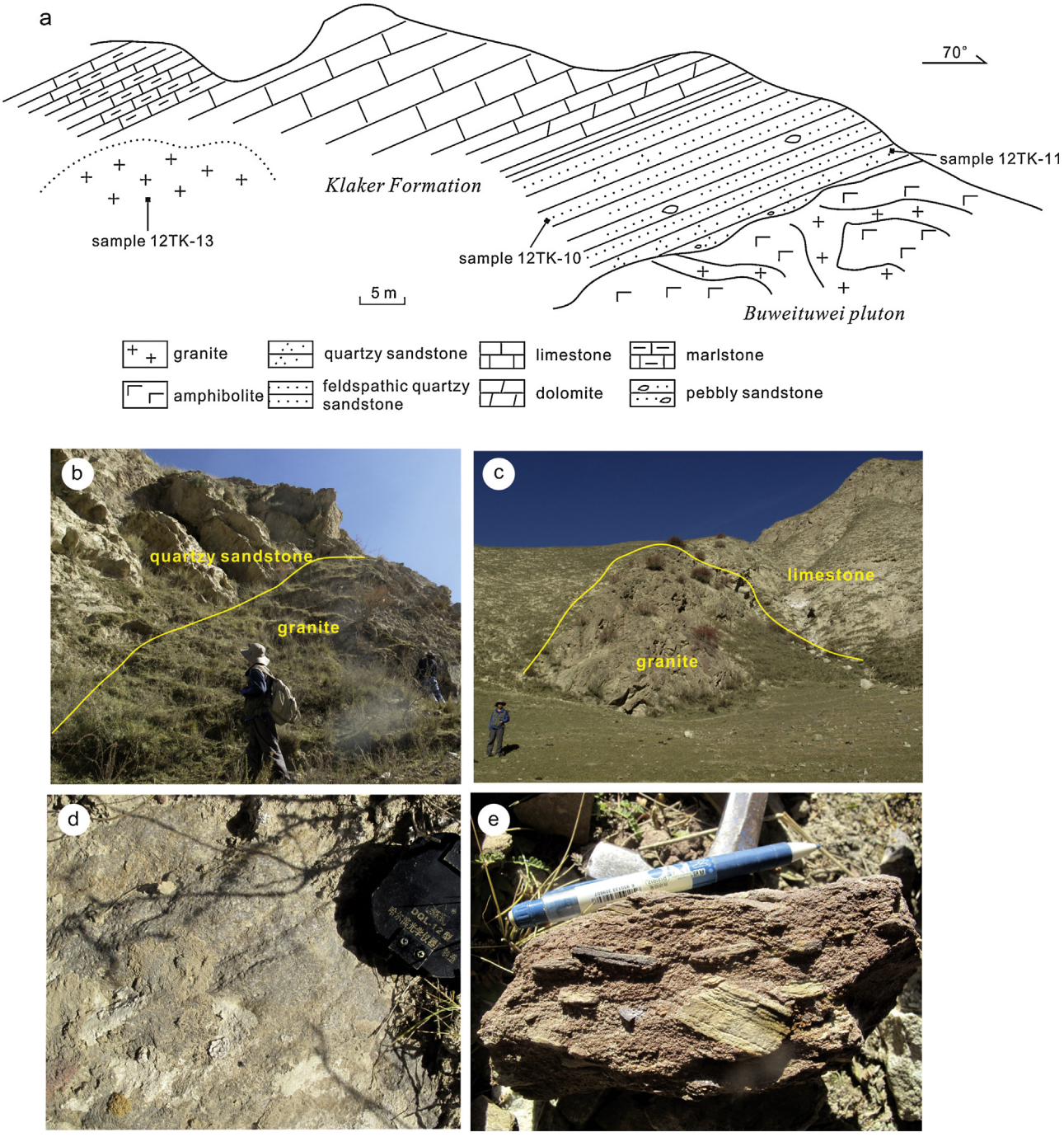

Fig. 4. Photographs of outcrops that illustrate the main lithologies in the Kuleakazi area: (a) Interpreted geological cross-section across the contact between the Buweituwei pluton and the overlying sedimentary sequences, with schematic locations of the dated samples; (b and c) The Buweituwei pluton nonconformity with the overlying sedimentary sequences; (d) Gray quartz sandstone from the sedimentary sequences; (e) purple feldspathic quartz sandstone from the sedimentary sequences.

Bochatetage Formation. Wang et al. (2004) considered that the entire sequence was part of a Neoproterozoic continental rift succession exhibiting fluvio-lacustrine, lacustrine and restricted littoral settings. No direct geochronological data support a Neoproterozoic age for this sequence; however, in the Akazi area, the sequence contains a polymictic boulder bed at the base of the section along with an overlying limestone succession (now marble; Fig. 5a and b) from which a 797 ± 12 Ma youngest detrital zircon age was obtained (Wang et al., 2014). The coarse clasts within the conglomerate appear to be locally derived (Fig. 5c).

3. Sampling and analytical methods

In an effort to provide tighter age constraints and to evaluate the provenance of sedimentary sequences within the Tiekelik Belt, we obtained U–Pb zircon ages from seven different samples. They were collected from the basal Heluositan Complex ($n = 2$), from the Buweituwei pluton ($n = 2$) and from overlying sedimentary sequences ($n = 3$; Table 1). In addition, major and trace elements for nine granite samples from the BP were analyzed. Table 1 is a list of the samples collected in this study

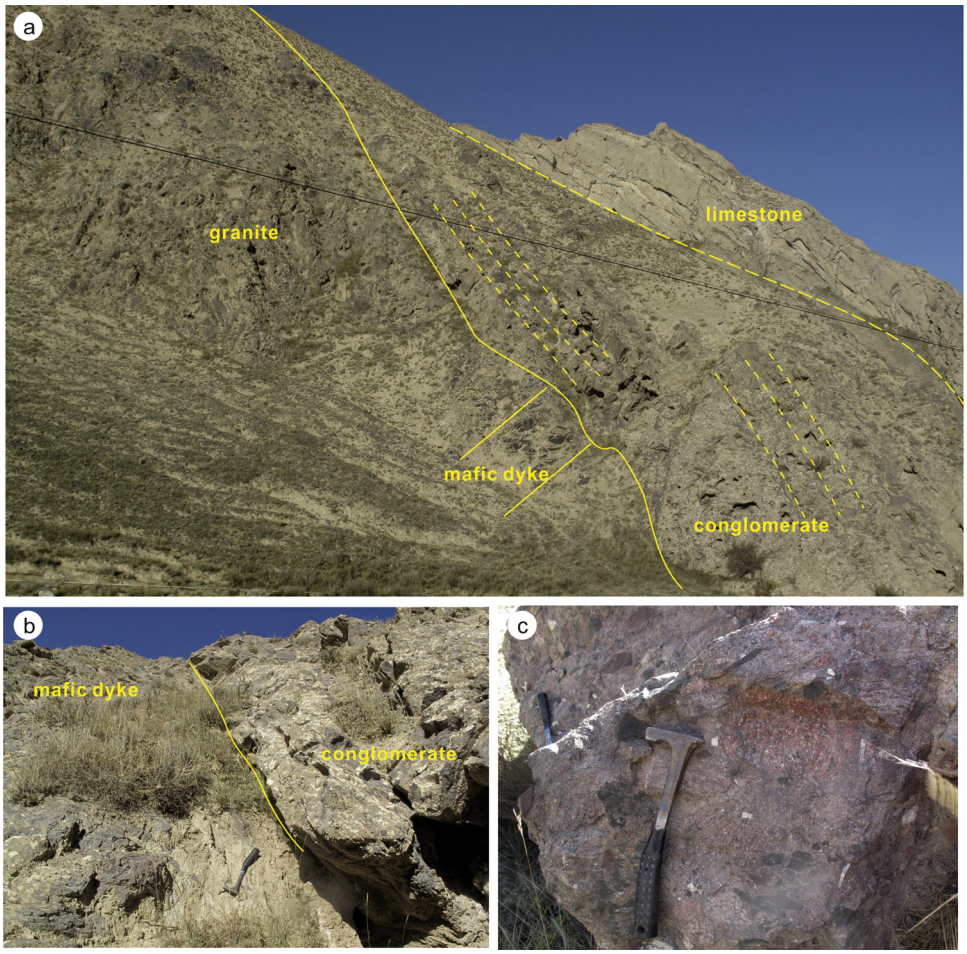

Fig. 5. Photographs of outcrops that illustrate the main lithologies in the Akazi area: (a) The contact between the Akazi pluton and overlying conglomerate; (b) the Akazi pluton nonconformably overlain by conglomerate; (c) variegated conglomerate.

along with the rock type, mineralogy, locality information and age results. Geochemical samples were analyzed at the State Key Laboratory of Continental Dynamics in Northwest University, Xi'an. Fresh chips of whole rock samples were powdered to a 200 mesh-size using a tungsten carbide ball mill. Major and trace elements were analyzed by XRF (Rikagu RIX 2100) and ICP-MS (Agilent 7500a), respectively. Analyses of USGS and Chinese national rock standards (BCR-2, GSR-1 and GSR-3) indicate that relative analytical precision and accuracy for major elements are generally better than 5%. For trace element analysis,

Table 1
Summary of sampling in this study.

Pluton/unit	Sample	Lithology	Locality	GPS position	Mineralogy	Ages (Ma ± 1σ)	Interpretation
Heluositan Complex	*07HL-51*	Quartz monzonite gneiss	20 km NW of Akazi Daban	N 37°7′21.4″ E76°49′55.5″	Quartz+feldspar+K-feldspar+biotite+amphibole	2329 ± 15 2257 ± 6 1832 ± 14	Inheritance Intrusion Metamorphic
	11XZ-8	Granitic gneiss	North side of Akazi Daban, 3 km W of Xinzang road	N37°5′45.7″ E76°57′16.5″	Quartz+feldspar+K-feldspar+biotite	2306 ± 10 2034 ± 51	Intrusion Metamorphic
Buweituwei pluton	*12TK-9*	Gneissic syenogranite	Kuleakazi, Qipan river	N37°23′40.3″ E76°34′31.7″	Quartz+feldspar+K-feldspar+biotite	1899 ± 10	Intrusion
	12TK-13	Biotite syenogranite	Kuleakazi, Qipan river		Quartz+K-feldspar+feldspar+biotite	1795 ± 32 Ma	Intrusion
Layileke Formation (?)	*11XZ-9*	Conglomeratic sandstone	North side of Akazi Daban, 1 km W of Xinzang road	N37°5′35.1″ E76°57′27.2″	Felsic, chert and spilite clast+Quartz+feldspar+K-feldspar+amphibole	1953 ± 9	Youngest detrital-zircon concordant age
Layileke Formation	*12TK-11*	Medium- to coarse-grained quartz sandstone	Kuleakazi, Qipan river		Quartz+feldspar+volcanic clast	1847 ± 7	
Layileke Formation	*12TK-10*	Medium- to coarse-grained feldspathic sandstone	Kuleakazi, Qipan river		Quartz+feldspar+calcite+clast	1779 ± 14	

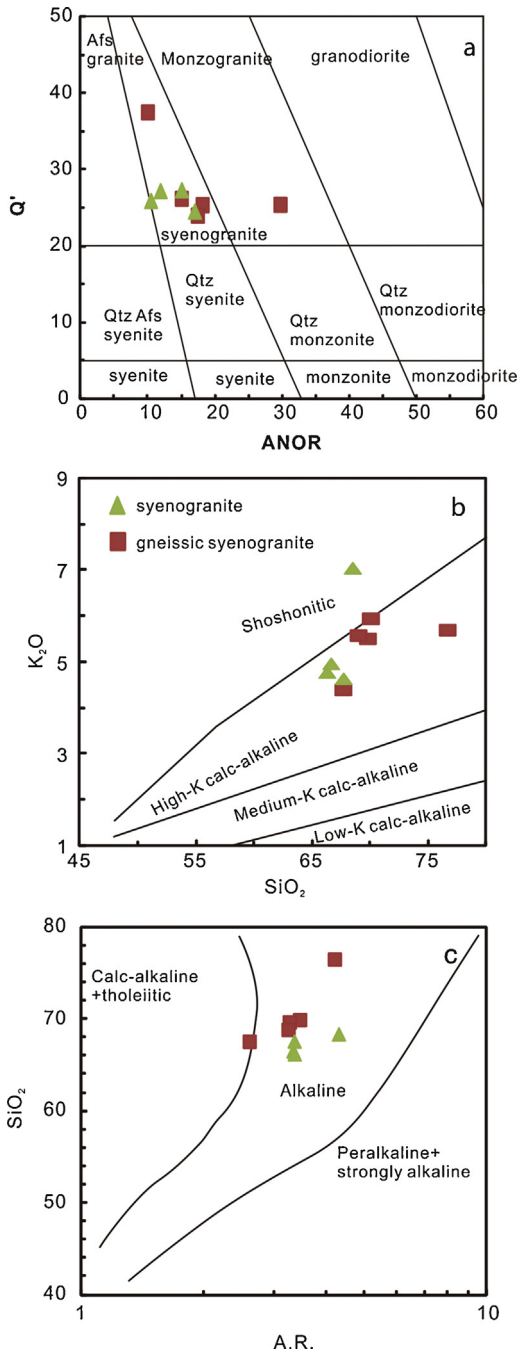

Fig. 6. Plot of Buweituwei granitic rocks on: (a) ANOR =100An/(Or + An) vs Q′ = 100Q/(Q + Or + Ab + An) diagram, after Streckeisen and Le Maitre (1979); (b) SiO_2 vs K_2O classification diagram with the boundary lines after Le Maitre (1989) and Rickwood (1989); (c) AR vs SiO_2 diagram (Wright, 1969) for the granites, where AR (alkalinity ratio) = $[Al_2O_3 + CaO + (Na_2O + K_2O)]/[Al_2O_3 + CaO - (Na_2O + K_2O)]$ (wt.%).

sample powders were digested using an HF + HNO_3 mixture in high-pressure Teflon bombs at 190 °C for 48 h. Relative analytical precision is better than 10% for most trace elements. The geochemical data are listed in Table 2 and Figs. 6 and 7.

Zircon grains were separated from the samples by heavy-liquid and magnetic techniques followed by hand picking under a binocular microscope. Zircon grains were mounted in epoxy resin discs, and then polished and coated with carbon. Cathodoluminescence (CL) images of the zircons were taken using a Mono CL3+ microprobe prior to U–Pb dating at the State Key Laboratory of Continental Dynamics at Northwest University, China, using an Agilent 7500a ICP-MS. The ICP-MS was equipped with a unique shield torch that yields higher sensitivity. The GeoLas 200M laser ablation system consists of a ComPex102 193 nm ArF-excimer laser (Lambda Physik) and optical system (MicroLas). During analysis, the spot diameter was 33 μm. ICP-MS operating conditions were generally optimized using continuous ablation of reference glass NIST SRM 610, to provide maximum sensitivity for the high masses while maintaining low oxide formation and low background. U, Th and Pb concentrations were calibrated by using ^{29}Si as the internal standard and NIST SRM 610 as the external standard. $^{207}Pb/^{206}Pb$ and $^{206}Pb/^{238}U$ ratios were calculated using the GLITTER 4.0 program, and then corrected using the Harvard zircon 91500 as the external standard. U–Pb ages were calculated using the ISOPLOT program (Ludwig, 2003). The detailed instrumental parameters and analytical procedures can be found in Yuan et al. (2004). The U–Pb data for the selected analyses are listed in Table 3 (Supplementary data). Data are illustrated on U–Pb concordia diagrams (Figs. 8–10) and relative probability plots (with a concordance in the range 90–110%) are provided in Fig. 10. Age probability diagrams were constructed using AgeDisplay (Sircombe, 2004). Zircon grains that exhibited 10% or less discordance are used in our analyses for interpretation of detrital zircon age.

4. Results

4.1. Major and trace element geochemistry

The Buweituwei granites from the Kuleakazi area are predominately classified as syenogranites according to Streckeisen and Le Maitre (1979; Fig. 6). SiO_2 concentrations for the syenogranites range from 66 to 77 wt.% (Table 2 and Fig. 6b). In the K_2O vs SiO_2 discrimination diagram (Fig. 6b), the syenogranites dominantly plot in the high-K calc–alkaline field. Using the classification of Wright (1969) the BP rocks plot primarily in the alkaline field (Fig. 6c). The REE patterns are highly fractionated (Fig. 7a). The La_N/Yb_N ratios vary between 23 and 146 and the samples exhibit neutral to markedly negative Eu anomalies (Fig. 7a). Samples show relative enrichment in the Large Ion Lithophile Elements (LILE – especially Rb, Ba and Th), with strong negative Ta, Nb and Sr anomalies (Fig. 7b). The FeOT/MgO vs 10,000 * Ga/Al and $(K_2O + Na_2O)/CaO$ vs Zr + Nb + Ce + Y discrimination plots of Whalen et al. (1987) place the samples within (or near) the A-type granite field (Fig. 7c and d).

4.2. Zircon geochronology

4.2.1. Heluositan Complex

Sample 07HL-51, quartz monzonite gneiss (Table 1): The CL images for sample 07HL-51 indicate complexly zoned zircon grains, many of which reveal core, mantle and rim structures (Fig. 8a). Bright relict cores without oscillatory zoning are labeled 'rc' in Fig. 8a. Magmatic cores showing either weak oscillatory zoning or patchy patterns are labeled 'c' in Fig. 8a. Some of the oscillatory cores within the zircons are locally transgressed by more luminescent, irregularly shaped patches of faintly banded zircon (Fig. 8a). The mantle domains of zircons have a dark CL response and no discernible internal structure (labeled 'm' Fig. 8a). Some rims show gray patchy patterns, and either follow or transect former zircon zoning patterns (labeled 'r_1' Fig. 8a). In a few grains, a very small brightly luminescent rim marks the grain edge (labeled 'r_2' Fig. 8a). These bright rims are noted for reference only as they are too narrow (<10 μm) for LA-ICP-MS analysis.

A total of 49 U–Pb spot analyses from 28 grains were carried out on different zircon domains (Table 3; Fig. 8b). Nine analyses of relict cores have U contents of 100–1636 ppm, Th contents of 49–642 ppm and Th/U ratios of 0.34–1.27 (Table 3). They yielded

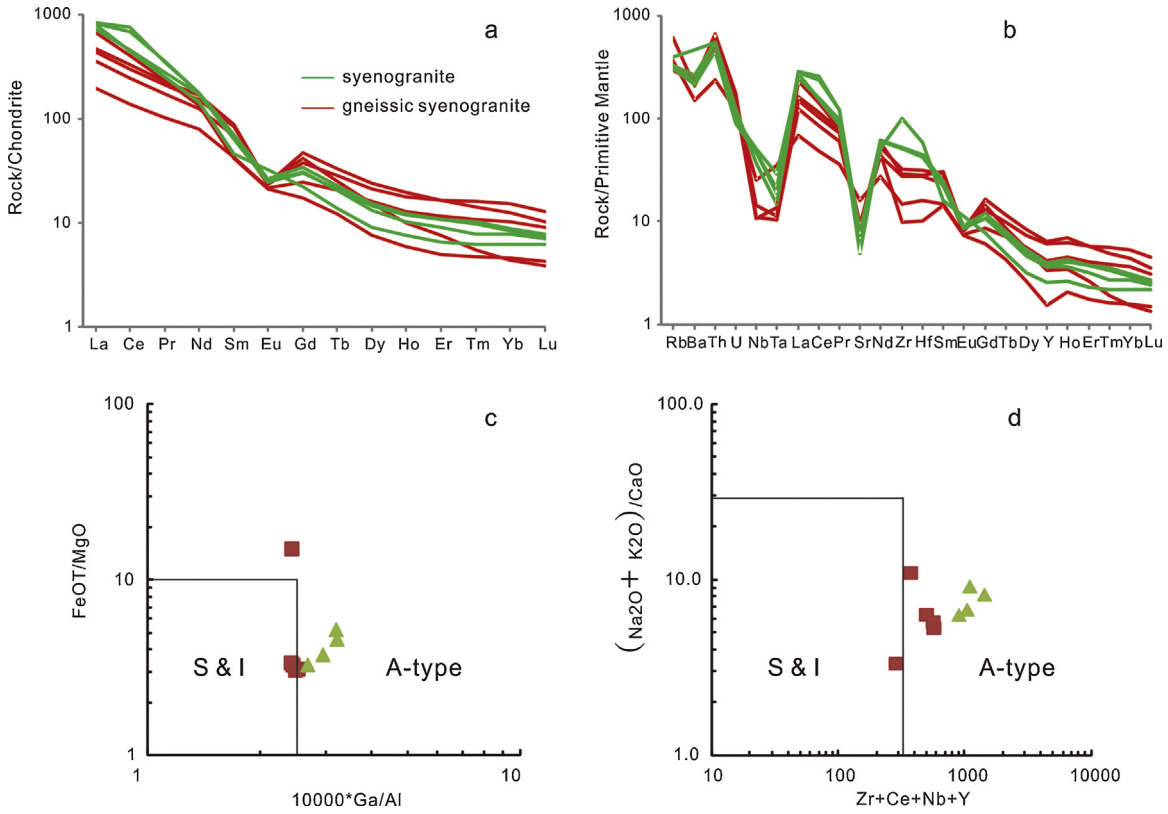

Fig. 7. (a and b) Chondrite normalized REE diagram and primordial mantle normalized trace element diagram showing the granitic rocks of the Buweituwei pluton. Normalizing chondrite and primordial mantle values are after Sun and McDonough (1989). (c and d) FeOT/MgO vs 10,000 * Ga/Al and $(K_2O + Na_2O)/CaO$ vs Zr + Nb + Ce + Y discrimination diagrams for the granitic rocks, after Whalen et al. (1987). Symbols as in Fig. 6.

$^{207}Pb/^{206}Pb$ ages ranging from 2364 to 2309 Ma (Fig. 8b). A total of 26 analyses were made on cores with a magmatic appearance. These show a large variation in their U and Th contents (80–451 and 39–270 ppm, respectively) and Th/U ratios (0.17–1.29). Ages from those samples yielded $^{207}Pb/^{206}Pb$ ages between 2285 Ma and 2132 Ma (Table 3; Fig. 8c). Six concordant analyses from 6 grains record a weighted mean $^{207}Pb/^{206}Pb$ age of 2257 ± 6 Ma (MSWD = 0.28) that is interpreted as the crystallization age of the granite protolith. The remaining core analyses are discordant, either reflecting single or multiple partial Pb loss, and/or new zircon growth followed by Pb-loss. Three mantle analyses gave discordant ages between 2002 Ma and 1987 Ma. Eleven analyses on rims have U and Th contents and Th/U ratios ranging from 54 to 1392 ppm, 10–533 ppm and 0.10–1.02, respectively and gave $^{207}Pb/^{206}Pb$ ages between 1853 and 1816 Ma (Table 3). Four concordant analyses from 4 grains yielded a weighted mean $^{207}Pb/^{206}Pb$ age of 1832 ± 14 Ma (MSWD = 0.48; Fig. 8d).

Sample 11XZ-8, *granitic gneiss* (Table 1): CL images of zircons from sample 11XZ-8 show gray luminescent, oscillatory zoning or faint cores surrounded by dark luminescent, unzoned or faintly banded rims (Fig. 8e). A total of 24 analyses from 20 grains were conducted on zircons from this sample (Table 3), including 18 analyses from cores and 6 analyses from rims. The U content of the cores ranges from 175 to 913 ppm, whereas the content in the rims ranges from 399 to 1080 ppm. Thorium concentrations based on core analyses ranging from 65 to 313 ppm and rims from 34 to 231 ppm. Th/U ratio for core analyses range from 0.07 to 0.74, whereas the Th/U ratios in the rims range from 0.03 to 0.29 (Table 3). The analyses define two distinct clusters (Fig. 8f). Eleven of the 18 core analyses plot close to concordia with $^{207}Pb/^{206}Pb$ ages ranging from 2425 to 2257 Ma, and define a weighted mean $^{207}Pb/^{206}Pb$ age of 2306 ± 10 Ma (MSWD = 3.1) that is interpreted as the crystallization age (Fig. 8g). Three of the 6 rim analyses gave concordant ages between 2040 Ma and 2007 Ma (Fig. 8h), that reflect the timing of metamorphic rim growth.

4.2.2. Buweituwei pluton

Sample 12TK-9, *gneissic syenogranite* (Table 1): The majority of zircons from this sample are prismatic with blunt pyramidal terminations. In CL images, they have all thick sector zoned cores and thin euhedral weakly zoned rims that were too narrow for analysis (Fig. 9a). Twenty-two analyses from the cores have U contents of 159–2919 ppm, Th contents of 67–1359 ppm and Th/U ratios of 0.22–1.30 (Table 3). They range from concordant to highly discordant, and lie along a discordia with an upper intercept age of 1896 ± 16 Ma (MSWD = 3.1; Fig. 9b). Eight of these points are concordant, and yield a concordia age of 1899 ± 10 Ma (Fig. 9b). We interpret the c. 1.9 Ga age as the time of intrusion for the syenogranite. The remaining spot analyses are discordant, reflecting partial Pb loss.

Sample 12TK-13, *biotite syenogranite* (Table 1): Sample 12TK-13 contained zircons with gray, well-developed oscillatory zoning (Fig. 9a). Seventy analyses have U contents of 452–1345 ppm, Th contents of 150–782 ppm and Th/U ratios of 0.14–1.20. The $^{207}Pb/^{206}Pb$ ages were dispersed much more than expected from the analytical uncertainties, indicative major radiogenic Pb loss, perhaps in several steps. Two zircon spots yield a concordant U–Pb age of 1795 ± 32 Ma (MSWD = 0.51; Fig. 9b) that is the best estimate for the crystallization age of this sample.

4.2.3. Sedimentary sequences

Sample 11XZ-9, *conglomeratic sandstone*, *Layileke Formation* (Table 1): Most zircon grains from sandstone sample 11XZ-9 are prismatic or rounded crystals, 150–300 μm in length. CL images

reveal gray oscillatory zoning (Fig. 10a) typical of magmatic grains. Fifty zircons were less than 10% discordant. The grains have U values between 84 and 633 ppm, Th values between 150 and 1152 ppm and Th/U ratios between 1.05 and 2.96 (Table 3). A wide range of $^{207}Pb/^{206}Pb$ ages was obtained from this samples spanning from 2400 to 1900 Ma, with the dominant population falling between 2400 and 2250 Ma (Fig. 10b and c). The youngest analyzed zircon yielded a concordant $^{207}Pb/^{206}Pb$ age at 1953 ± 9 Ma (Fig. 10b).

Sample 12TK-11, *quartz sandstone*, *Layileke Formation* (Table 1): The zircons are commonly 100–200 μm in size, round or prismatic in shape, and show oscillatory zoning in CL (Fig. 10a). Some grains show clear core–rim structures in CL images (Fig. 10a). U–Pb age data from 79 spots from 79 grains with discordance less than 10% were selected for statistical interpretation. U, Th contents and Th/U ratios range from 56 to 775 ppm, 27 to 505 ppm and 0.15 to 1.71, respectively (Table 3). Most analyses were spread along the concordia from 2300 to 1800 Ma (Fig. 10b), with distinct peaks at 1870, 2120, 2210 and 2270 Ma (Fig. 10c). The youngest zircon has an age of 1779 ± 14 Ma (97% concordance).

Sample 12TK-10, *feldspathic sandstone*, *Layileke Formation* (Table 1): The zircons are small in size (commonly c. 100 μm) and round or stubby in shape, and show oscillatory zoning or homogeneous structures with secondary (metamorphic) rims in CL (Fig. 10a). A total of 32 analyses from 32 different grains yielded useful data. U and Th contents and Th/U ratios show large variations from 12 to 454 ppm, 1 to 1475 ppm and 0.16 to 1.73, respectively (Table 3). Many analyses show lead loss, but two broad age peaks are clear at c. 1900 Ma and c. 2300 Ma (Fig. 10b and c). The youngest, and least discordant (c. 2%) zircon yielded an age of 1847 ± 7 Ma (Fig. 10b).

5. Discussion

5.1. Ages of the metamorphic and magmatic rocks

Zircon from the Heluositan Complex sample 07HL-51 defines three age clusters: c. 2365–2310 Ma, c. 2260 Ma and c. 1830 Ma (Table 3 and Fig. 8). The 2365–2310 Ma grouping was obtained from small rounded inherited cores. We conclude that these are most likely inherited grains derived from a crustal component in the source. $^{207}Pb/^{206}Pb$ ages of around 2260 Ma obtained from oscillatory or sector zoned zircon cores are interpreted to reflect the crystallization age of the granitic gneiss protolith. Resetting of the U–Pb system during metamorphism, as indicated by U-enrichment, dissolution features and erosional surfaces, are reflected in the 1830 Ma age obtained from zircon rim analyses (Fig. 8a). The zircon mantles from sample 07HL-51 have low Th concentrations (70–86 ppm). In the CL images, the interface between mantle and core show an irregular erosion surface (Fig. 8a) suggestive of dissolution of existing zircon and precipitation of new zircon (e.g. Grant et al., 2009). Zircon rims in 07HL-51 show both U enrichment relative to the cores and have variable Th/U ratios, and are interpreted as having grown in the presence of fluids during regional metamorphism (e.g. Corfu et al., 2003; Möller et al., 2003; Grant et al., 2009). This interpretation is supported by the apparent fluid interaction observed in the zircon (Fig. 8a). Ages from core–rim interfaces may represent mixed ages between the core and rim, and an unambiguous interpretation is not possible on the basis of the combined CL and U–Pb dataset.

Sample 11XZ-8 yields ages of c. 2310 and 2040–2007 Ma (Table 3 and Fig. 11). The older ages are similar to those of the 2.3 Ga Buweiduwei granites (Zhang et al., 2007). As a result, we consider the average $^{207}Pb/^{206}Pb$ age of 2310 Ma as the crystallization age for this granitic gneiss protolith. The younger $^{207}Pb/^{206}Pb$ ages are more scattered, but our best estimate is that the c. 2.03–2.00 Ga ages reflect the age of metamorphism in this sample. This is slightly older than the 1.9 Ga metamorphic age from the Akazi pluton reported by Zhang et al. (2007).

Sample 12TK-9 from the BP pluton gives a well-constrained concordia age of 1899 ± 10 Ma that is considered to be the intrusion age. Sample 12TK-13 displays a limited scatter of individual $^{207}Pb/^{206}Pb$ ages around 1795 Ma, which we interpret as the age of emplacement for a distinct younger phase of intrusive activity within the pluton. All these ages are younger than the U–Pb age of 2340 Ma previously published by Zhang et al. (2007). The age of the potassic granite suite reported by Zhang et al. (2007) is similar to our age for the granitoid gneisses of the Heluositan Complex (2.3–2.2 Ga). Therefore, we speculate that the potassic granite suite reported by Zhang et al. (2007) might belong to the Heluositan Complex. It would also appear that the Buweituwei 'pluton' does not represent a single magmatic body given the range in ages reported here (1900–1795 Ma). Given this conclusion regarding the BP and the fact that the age of the AP (2.4 Ga) is older than the granitoid gneisses of the Heluositan Complex (2.3–2.2 Ga). A major revision of the Paleoproterozoic basement terminology might be required. At the very least, additional geochronologic studies in the region are warranted.

5.2. Source of the Paleoproterozoic Buweituwei magmatism

Geochemical features of the Buweituwei syenogranite are indicative of A-type magmatism. Mechanisms proposed for the genesis of A-type granitoids include the differentiation of mantle-derived magmas (e.g. Loiselle and Wones, 1979; Eby, 1990; Turner et al., 1992; Frost and Frost, 1997; Bonin, 2007), the partial melting of felsic granulites (e.g. Collins et al., 1982; Clemens et al., 1986; Whalen et al., 1987) and partial melting of an intermediate crustal source (Anderson, 1983; Creaser et al., 1991; Skjerlie and Johnston, 1992; Patiño Douce, 1997).

The BP syenogranites are characterized by high SiO_2, Rb, Th and HREE concentrations but low Mg-number, Sr/Y, and Ti contents and Rb/Sr ratios, indicating that they were not derived by partial melting of lower crust. The low abundances of Sr in the rocks and the presence of negative Eu anomalies reflect the presence of residual plagioclase and K-feldspar in the source (e.g. Harris and Inger, 1992). In the $Al_2O_3/(FeO + MgO + TiO_2)$ vs $Al_2O_3 + FeO + MgO + TiO_2$ diagram, these rocks plot in the field of greywacke-derived melts and amphibolite-derived melts (Fig. 11a).

Experimental results suggest that partial melting of tonalitic to granodioritic compositions can produce some A-type granitoid magmas (Patiño Douce, 1997; Skjerlie and Johnston, 1993; Bogaerts et al., 2006). Using the classification of Frost et al. (2001), the BP syenogranites belong to the ferroan and magnesian series (Fig. 11b). On the modified alkali–lime index (MALI = $Na_2O + K_2O - CaO$ by wt) diagram (Fig. 11c), the BP samples plot in the alkalic and alkalic–calc field with one exception that fell within the calc–alkalic field. The data shown in Fig. 11 suggest that, apart from a few examples, most BP syenogranites likely formed by partial melting of a ferroan granodiorite. However, some samples of the BP syenogranites show ferroan, alkali and peraluminous compositions. The experiments predict that partial melting of tonalitic to granodioritic crust produces alkali–calcic to calc–alkalic granitoids that are metaluminous at low pressures and peraluminous at high pressures (Frost and Frost, 2011). Therefore, we argue that the BP peraluminous syenogranites might be produced by partial melting of ferroan granodiorite over 4 kbar (Bogaerts et al., 2006).

5.3. Sedimentary rocks

The three youngest concordant detrital zircons from the overlying sedimentary sequence yielded ages of 1779 ± 14 Ma,

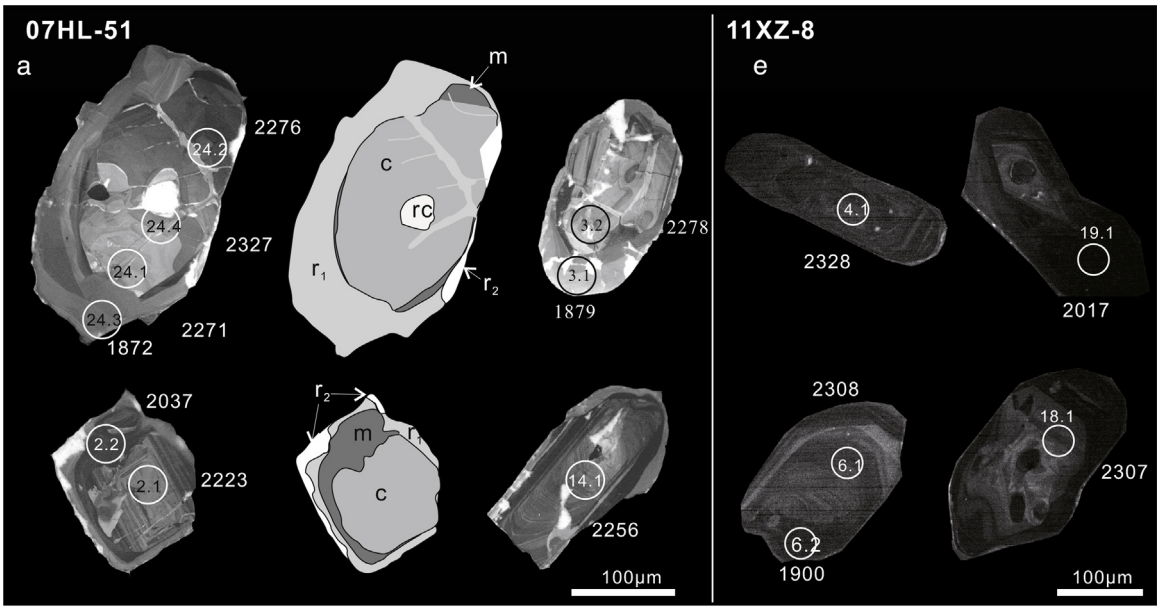
07HL-51
a
2276
24.2
24.4
2327
24.1
24.3
1872
2271
m
c
rc
r1
r2
3.2
2278
3.1
1879
2037
2.2
2.1
2223
r2
m
r1
c
14.1
2256
100μm
11XZ-8
e
4.1
2328
19.1
2017
2308
6.1
6.2
1900
18.1
2307
100μm

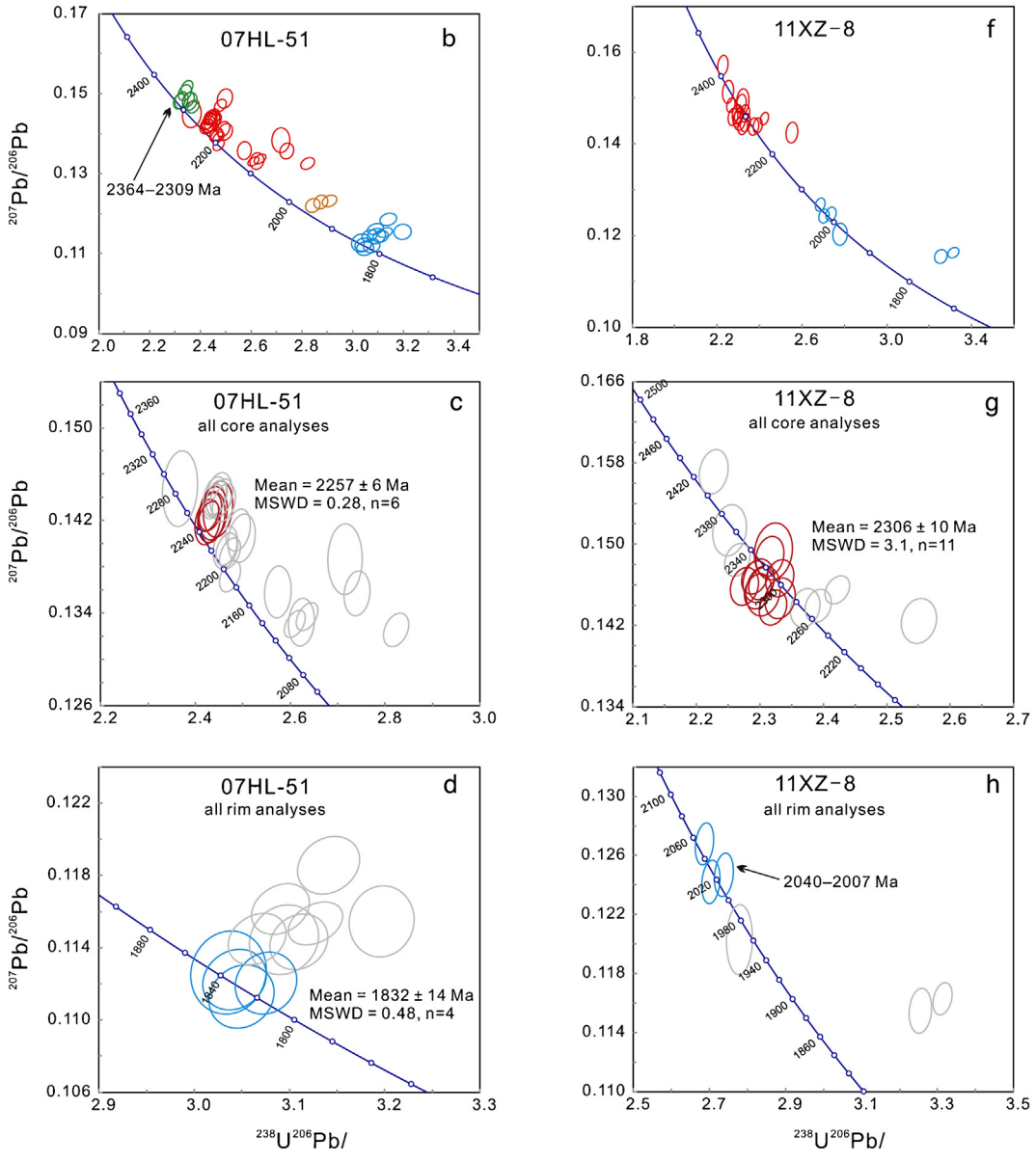
07HL-51
b
2364–2309 Ma
11XZ-8
f
07HL-51
all core analyses
c
Mean = 2257 ± 6 Ma
MSWD = 0.28, n=6
11XZ-8
all core analyses
g
Mean = 2306 ± 10 Ma
MSWD = 3.1, n=11
07HL-51
all rim analyses
d
Mean = 1832 ± 14 Ma
MSWD = 0.48, n=4
11XZ-8
all rim analyses
h
2040–2007 Ma
207Pb/206Pb
238U206Pb/

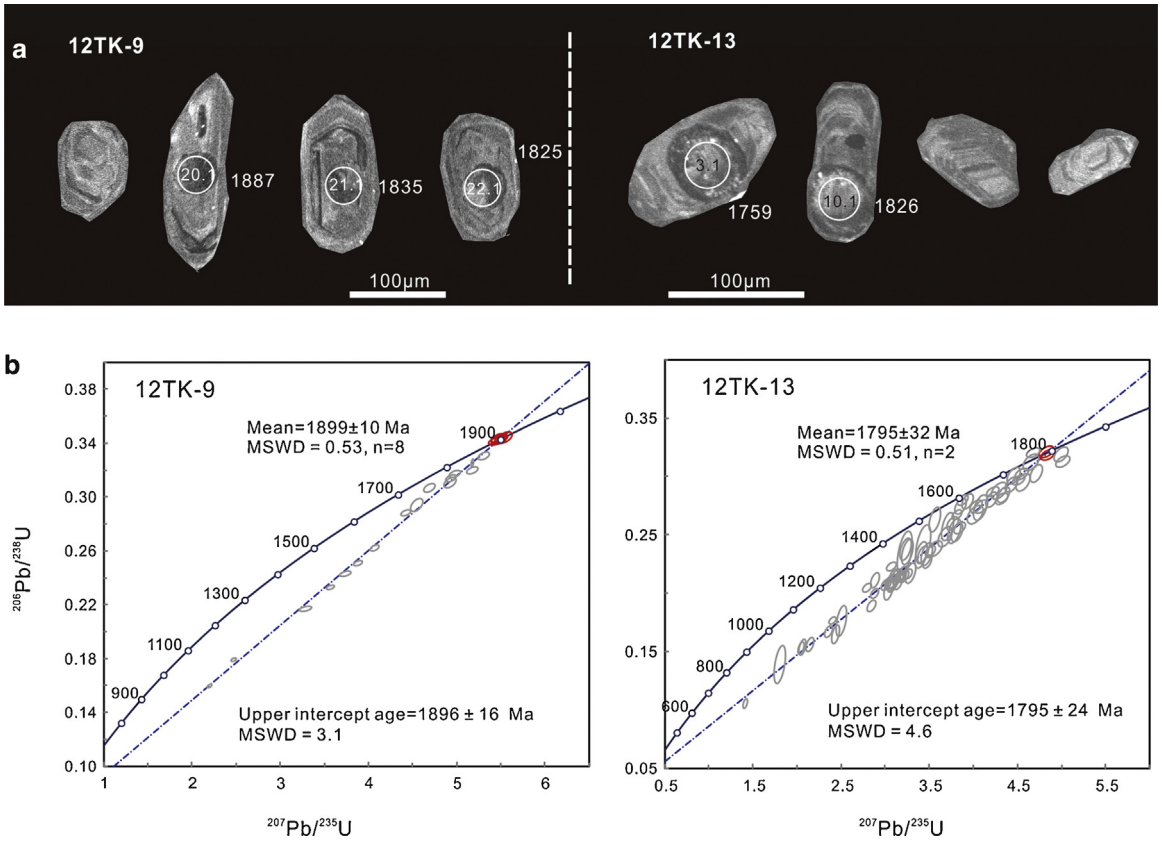

Fig. 9. (a) Cathodoluminescence images of selected zircons from samples of the Buweituwei pluton. The circles represent the position of laser spots used for age determination, with spot number and $^{207}Pb/^{206}Pb$ age (in Ma). (b) Conventional concordia diagrams for the zircon data obtained. The concordant analyses in red are included in the weighted mean. (For interpretation of the references to color in text, the reader is referred to the web version of this article.)

1847 ± 7 Ma and 1953 ± 9 Ma. Since the sedimentary sequence overlies the 1899–1795 Ma polyphase BP intrusions and the metamorphosed Akazi granite (1916 ± 7 Ma; Zhang et al., 2007), the depositional ages must be less than 1779 Ma. Unfortunately, more stringent constraints on these rocks cannot be determined and the age of deposition can only be constrained to between 1779 and 797 Ma (Wang et al., 2014).

Detrital zircon age probability diagrams for sample 12TK-10 and 12TK-11 (Fig. 10c) have major peaks around 1900–1800 Ma and 2400–2200 Ma, while zircon ages from sample 11XZ-9 range between 2400 and 2100 Ma, and zircons in the 1900–1800 Ma range are scarce. The detrital zircon data suggest local derivation of the zircons, with significant sample-to-sample variability. Igneous rocks dated between 2300 and 1800 Ma are present in the Tiekelik Belt and include the Heluositan Complex, and the Buweituwei and Akazi granitoid rocks (Xu and Zhang, 1996; Zhang et al., 2007; this study). The closest source region for zircons in the sample 11XZ-9 is from the Akazi granitoids, that are about 50 km to the SE of the sample site at Kuleakazi.

5.4. Archean–Proterozoic tectonic implications for the Tarim craton (southwestern margin)

Based on our results and previous studies, the Archean–Proterozoic evolution of the Tiekelik Belt along the southwestern margin of the Tarim Craton can be divided into four successive events, that are highlighted in Fig. 12 and can be summarized as follows:

(1) *3.14–2.76 Ga:* Guo et al. (2013) reported a protolith age of 3140 Ma for a granitic gneiss from the Heluositan Complex. Geochemical data from those gneisses show a TTG affinity (Guo et al., 2013). Nd and Hf isotopic studies (Zhang et al., 2007; Wang et al., 2009) have shown that Archean crust formation in the Tiekelik Belt took place between 3.17 and 2.76 Ga. Zhang et al. (2007) documented that the 2.41 Ga granodiorite–adamellite suite have Nd model ages (T_{2DM}) between 3.17 Ga and 3.05 Ga, and that the 2.34 Ga suite have narrow T_{2DM} ranges (2.91–2.76 Ga). Wang et al. (2009) reported that the 2330 Ma relict zircon cores from sample 07HL-51 have a $\varepsilon Hf(t)$ range from −0.8 to −3.4 and Hf model age of 2925–2800 Ma. This stage might be related to the formation of proto continental crust (TTG) before 3.0 Ga.

(2) *2.41–2.26 Ga:* This age range is reflected in the crystallization ages from samples 07HL-51 and 11XZ-8 along with the age of inherited zircons from sample 07HL-51. Moreover, detrital zircons from the sedimentary rocks record several age peaks at c. 2400–2200 Ma (Fig. 10c). Together with previous work by Xu and Zhang (1996) and Zhang et al. (2007), the evidence points to a major episode of magmatism at c. 2.41–2.26 Ga in the Tiekelik

Fig. 8. Cathodoluminescence images and schematic drawings of zircons from the sample 07HL-51 (a) and 11XZ-8 (e) and Tera–Wasserburg concordia diagrams of zircon data from granodiorite gneiss sample 07HL-51 (b–d) and from granitic gneiss sample 11XZ-8 (f–h). The circles represent the position of laser spots used for age determination, with spot number and approximate $^{207}Pb/^{206}Pb$ age (in Ma). Marked internal grain structures include relict cores (rc), cores (c), mantle (m), rims (r_1) and outer rim (r_2). Green ellipses = relict core analyses; red ellipses = core analyses; orange ellipses = mantle analyses; blue ellipses = rim analyses, the analyses in gray are not included in the weighted mean. (For interpretation of the references to color in text, the reader is referred to the web version of this article.)

Table 2
Major- and trace-element analytical data.

Sample type	12TK-9 (1)	12TK-9(2)	12TK-9(3)	12TK-9(4)	12TK-9(5)	12TK-13(1)	12TK-13(3)	12TK-13(4)	12TK-13(5)
	Gneissic syengranite					Syengranite			
SiO_2	70.0	69.7	67.6	68.9	76.6	68.5	66.6	66.3	67.7
Al_2O_3	15.1	15.2	15.6	15.8	12.9	14.2	14.4	14.7	15.0
Fe_2O_3T	2.1	2.2	2.7	2.3	1.3	3.0	4.6	4.9	4.1
CaO	1.4	1.7	2.4	1.6	0.8	1.2	1.2	1.4	0.9
MgO	0.6	0.6	0.8	0.6	0.1	0.8	1.1	0.9	0.8
K_2O	6.0	5.5	4.4	5.6	5.7	7.1	5.0	4.8	4.6
Na_2O	3.1	3.4	3.5	3.5	2.7	2.5	3.4	3.9	4.0
MnO	0.0	0.0	0.1	0.0	0.0	0.0	0.0	0.0	0.0
TiO_2	0.4	0.4	0.4	0.4	0.0	0.5	0.6	0.6	0.6
P_2O_5	0.1	0.2	0.1	0.1	0.0	0.1	0.2	0.2	0.2
LOI	0.8	1.0	2.2	0.9	0.4	2.0	2.6	2.2	1.9
Total	99.9	100.1	99.9	99.9	100.7	99.9	99.9	99.9	99.9
Li	11.3	12.9	20.9	11	5.75	11.6	16.7	13.1	14.1
Be	1	0.97	4.21	0.99	2.5	1.14	1.5	2.28	2.41
Sc	2.41	1.76	4.01	2.44	0.22	1.93	7.4	5.8	5.08
V	22.2	24.1	14.6	24.6	2.23	19.2	35.2	37.3	33.4
Cr	155	159	110	143	201	123	132	115	155
Co	6.02	6.62	4.38	5.73	1.94	5.84	7.94	6.9	7.09
Ni	7.4	8.14	4	7.66	6.84	7.92	7.12	8.72	7.22
Cu	1.12	2.21	3.62	1.59	4.78	4.39	2.84	4.78	4.01
Zn	39.2	50.4	124	32.3	46	87.2	76.6	92.7	98.8
Ga	19.6	20.3	20.5	20.2	16.6	20.2	22.5	24.9	25.6
Ge	1.02	0.98	1.14	0.97	0.82	1.04	1.4	1.21	1.22
Rb	207	205	232	188	392	255	200	191	209
Sr	180	190	336	184	196	143	104	153	160
Y	27.5	15.4	19	28.9	6.98	11.7	16.3	16.5	17.7
Zr	310	359	164	324	109	1120	574	566	584
Nb	7.81	10.3	18.2	7.76	7.58	26	33.2	36	33.2
Cs	0.8	0.78	4.78	0.7	2	0.53	0.78	0.66	0.79
Ba	1760	1780	1060	1610	1440	3280	1500	1640	1870
La	84.2	103	46.6	111	159	188	194	171	197
Ce	152	184	85.4	201	249	274	420	281	462
Pr	16.6	19.9	9.84	21.8	22.2	24.1	33.6	26.6	33.5
Nd	59.1	71	36.9	78	62.7	68.5	83.8	81.8	83.6
Sm	10.4	12.7	6.48	13.6	6.43	7.14	10.2	9.76	10.9
Eu	1.35	1.42	1.27	1.4	1.24	1.9	1.48	1.44	1.53
Gd	7.7	8.63	5.13	9.67	3.58	4.6	6.32	6.27	7
Tb	1.07	0.94	0.77	1.25	0.46	0.52	0.77	0.8	0.85
Dy	5.41	3.95	4.06	6.12	1.95	2.34	3.39	3.72	3.91
Ho	1.02	0.57	0.73	1.12	0.34	0.43	0.59	0.67	0.7
Er	2.75	1.26	1.93	2.77	0.83	1.1	1.5	1.8	1.8
Tm	0.41	0.14	0.28	0.36	0.12	0.16	0.2	0.26	0.25
Yb	2.62	0.75	1.77	2.16	0.78	1.06	1.34	1.51	1.45
Lu	0.33	0.099	0.23	0.26	0.11	0.16	0.18	0.2	0.19
Hf	8.4	9.57	4.93	8.69	3.16	17.9	13	13.4	13.6
Ta	0.42	0.46	1.45	0.42	0.55	0.6	0.76	1.2	0.85
Pb	47.2	46.6	40	47.7	48.3	16.4	10.8	11.3	9.84
Th	41.2	49.3	20.4	56.3	49.6	47	38.6	38.1	46.6
U	3.08	3.22	2.52	3.69	3.14	2.58	1.9	2.03	2.24
A/CNK	1.1	1.0	1.1	1.1	1.1	1.0	1.1	1.0	1.1
Eu/Eu*	0.15	0.14	0.22	0.12	0.26	0.33	0.18	0.18	0.18
$(La/Yb)_N$	23	99	19	37	146	127	104	81	97
Mg#	39.0	40.2	40.6	38.3	12.2	38.9	35.8	28.6	31.3

Belt. Negative εHf values (−0.8 to −3.4) in zircons from sample 07HL-51 (Wang et al., 2009), as well as negative $\varepsilon Nd(t)$ values from the 2.41 Ga Akazi and the 2.34 Ga Buweituwei granitoids (Zhang et al., 2007) indicate the recycled nature of this crust, with Archean sources. Geochemical and Nd isotopic data for 2.41–2.34 Ga granitoids suggests that the A and S-type granites might have been produced by partial melting of the Archean mafic crust, felsic pelites and/or metagreywackes that were recycled from Archean crust (TTG?) in a continental rift environment (Zhang et al., 2007).

(3) *2.03–1.80 Ga:* According to our age data and previous studies, the Proterozoic rocks of the Tiekelik Belt underwent several episodes of metamorphism at 2040–2007 Ma, 1920 and 1830 Ma. A-type granitoids formed by partial melting of an intermediate source were emplaced at 1900 and 1795 Ma ago in the BP and mafic dykes (1.9 Ga, unpublished data) were intruded into the Heluositan Complex. These extensional magmatic episodes may reflect continental lithospheric thinning between c. 1.9 and 1.8 Ga. Since these magmatic episodes are coeval with metamorphism, the evidence might support orogenic extension in the Tiekelik Belt during this interval (e.g. Wang et al., 2014). It is difficult to fully understand the exact nature of metamorphism and magmatic activity without establishing the *P–T* conditions and additional geochronological data, especially since we are apparently dealing either with a very prolonged period of magmatic and metamorphic activity (c. 250 million years), or several separate episodes.

(4) *Post-1.8 Ga:* Following the emplacement of intraplate-generated magmatic products between 1.9 and 1.8 Ga, the southwestern Tarim Craton entered a period of subsidence, leading to deposition of the sedimentary sequences in the Tiekelik Belt. The youngest detrital zircon grains from the

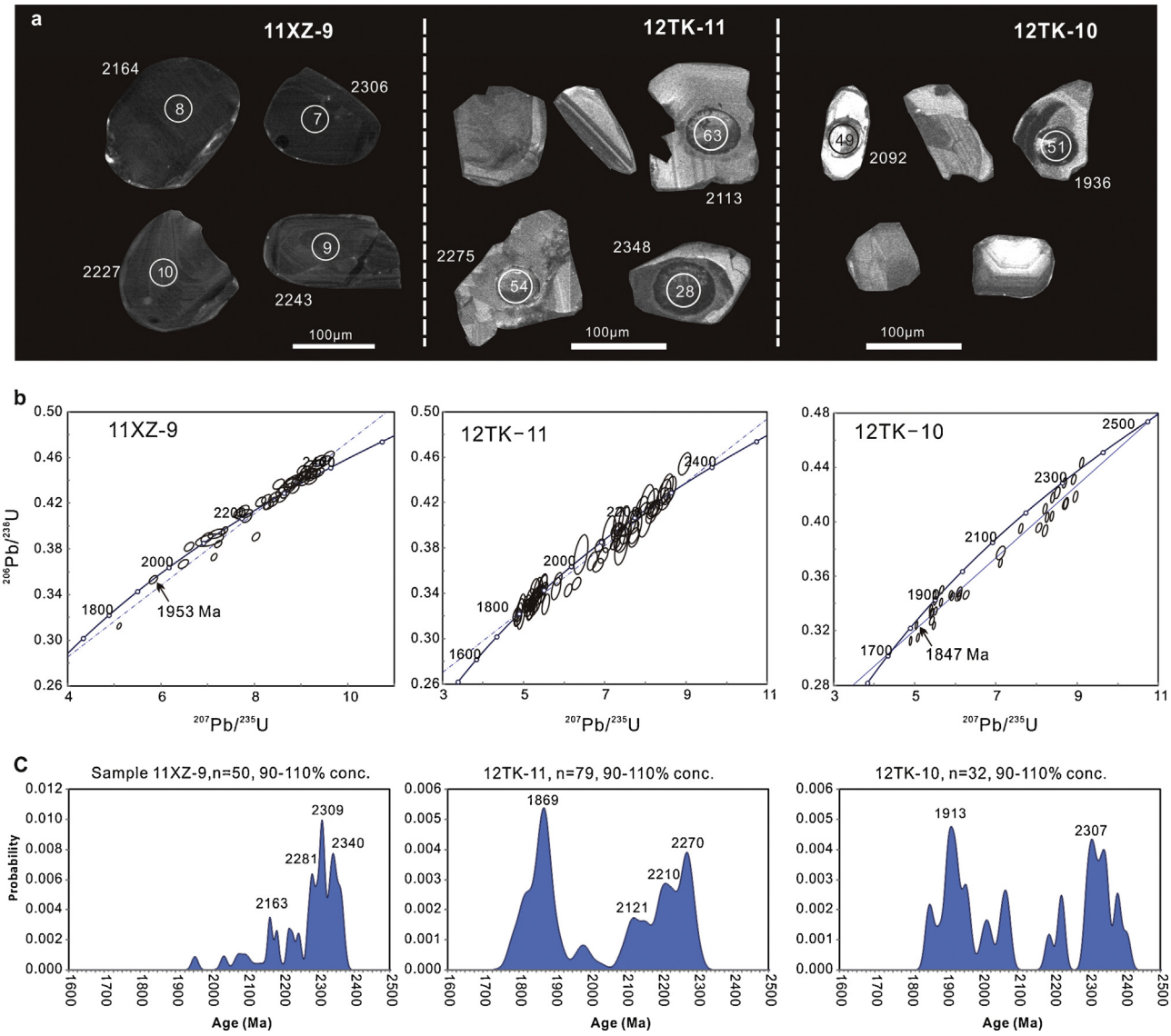

Fig. 10. (a) Cathodoluminescence images of selected zircons from samples of the Changcheng sedimentary sequences. The circles represent the position of laser spots used for age determination, with spot number and $^{207}Pb/^{206}Pb$ age (in Ma). (b) Concordia diagrams for the same samples. (c) Age probability diagrams for all 90–110% concordant analyses. *n*: number of analyses with 90–110% concordance.

sediments are 1.95–1.78 Ga, consistent with derivation from local basement rocks. The exact age of these sedimentary rocks and their association with the Changcheng (1.8–1.6 Ga), Jixian (1.6–1.4 Ga), or younger sequences must await more detailed geochronological and sedimentological investigations. However, the Changcheng succession is less metamorphosed (or unmetamorphosed) compared to the Neoproterozoic sequences. In addition, the Changcheng sediments contain locally derived Paleoproterozoic zircons, and no Meso- or Neoproterozoic aged zircons, suggesting they could well be Mesoproterozoic, and not at all belong to the Neoproterozoic sequences discussed in Wang et al. (2014).

5.5. Comparison with the North Altyn–Dunhuang block and Alashan block

The North Altyn–Dunhuang block in the southeastern margin of Tarim Craton, comprises a suite of Archean–Proterozoic rock units, and represents the basement of the southeastern margin of the Tarim Craton (RGXR, 1993; Li et al., 2001; Lu and Yuan, 2003; Che and Sun, 1996; Zhang et al., 2013b). The Precambrian rocks of the North Altyn–Dunhuang block includes the Aketashitage Complex, the Dunhuang Complex, the Milan Group, the Dunhuang Group, the Annanba Group and abundant Palaeoproterozoic mafic and felsic intrusions (BGMG, 1989; Lu et al., 2008; Xin et al., 2011). U–Pb zircon dating results indicate that the North Altyn–Dunhuang block comprises an Archean mafic granulite and felsic gneiss (TTG gneiss) with several stages of magmatic events at c. 2.9 Ga, c. 2.8 Ga, c. 2.7 Ga and c. 2.6–2.5 Ga (Gehrels et al., 2003; Lu et al., 2008; Xin et al., 2013; Zhang et al., 2013b; Zhao et al., 2013; Zong et al., 2013). The post-Archean evolution was characterized by the emplacement of granite (c. 2.4 Ga), basic dykes (c. 2.35 Ga) and granodiorite (c. 2.3), which were later metamorphosed to form granitic gneisses (Lu and Yuan, 2003; Lu et al., 2008; Zhang et al., 2013b). This was followed by the emplacement of granitoid plutons with ages of c. 2.1 Ga, c. 2.05 Ga, c. 1.87–1.85 Ga and c. 1.75–1.73 Ga (Gehrels et al., 2003; Xin et al., 2011; He et al., 2013), mafic rocks dated at c. 2.0 Ga and c. 1.8 Ga (Wang, 2011; Liu et al., 2012; He et al., 2013) and metamorphic and anatectic ages at c. 2.0 Ga and c. 1.9–1.82 Ga (Gehrels et al., 2003; Lu et al., 2008; Wang, 2011; Yang et al., 2012; Xin

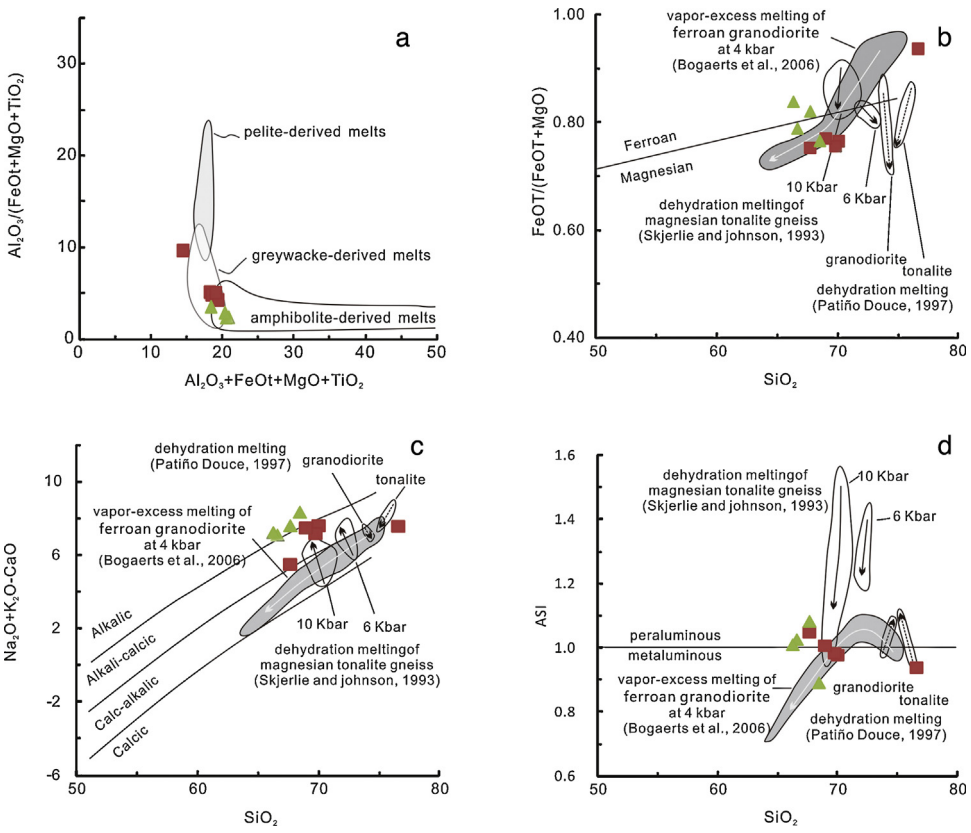

Fig. 11. (a) the $Al_2O_3/(FeO+MgO+TiO_2)$ vs $Al_2O_3+FeO+MgO+TiO_2$ after Patiño Douce (1999); (b) FeOT/(FeOT + MgO) vs SiO_2, boundary between ferrous and magnesian rocks from Frost and Frost (2008); (c) MALI vs SiO_2, boundaries between calcic, calc–alkalic, alkali–calcic and alkalic granitoids from Frost et al. (2001); (d) ASI [aluminum saturation index; Al/(Ca − 1.67P + Na + K)] vs SiO_2. Arrows show trends followed by the melt with increasing T (i.e. degree of melting) for Skjerlie and Johnston (1993) and with increased pressure (4 kbar at the tail of the arrow and 8 kbar at the arrow head) for Patiño Douce (1997). Like the results from Patiño Douce (1997) and Skjerlie and Johnston (1993), experiments by Bogaerts et al. (2006) produce mainly high-silica partial melts; only with high degrees of melting (>75% melt) do melt compositions decrease to less than 70% SiO_2.

et al., 2011, 2013; Zong et al., 2013; Zhang et al., 2012c, 2013b). These data (Fig. 12) suggest that the North Altyn–Dunhuang block experienced multistage crustal growth and reworking history during the Archean–Paleoproterozoic. The extensive geological and geochronological data indicating 2.1–1.7 Ga orogenesis may be related to the formation of the Columbia Supercontinent.

The Alashan block was traditionally considered to be part of the North China Craton (Ren et al., 1980; Wu et al., 1998; Zhai and Bian, 2000; Zhai and Santosh, 2011; Zhao and Zhai, 2012; Zhang et al., 2013a). The Precambrian rocks of the Alashan block include the Neoarchean–Paleoproterozoic Diebusige Group, the Bayanwulashan Group, the Boluositanmiao Complex, the Longshoushan Complex and the Beidashan Complex along with overlying Mesoproterozoic and Neoproterozoic sequences and abundant Palaeoproterozoic mafic and felsic intrusions (Geng et al., 2006, 2007; Xiu et al., 2002, 2004; Tung et al., 2007; Dan et al., 2012; Gong et al., 2011, 2012; Zhang et al., 2013a). Available U–Pb zircon geochronological data suggest a major episode of crustal growth at c. 2.8–2.7 Ga, followed by a c. 2.5 Ga magmatic–metamorphic event (Gong et al., 2012; Zhang et al., 2013a). Post-Archean magmatic ages from a variety of mafic and felsic igneous rocks are c. 2.3 Ga, c. 2.2 Ga and c. 2.0–1.9 Ga, respectively, followed by a c. 1.9–1.8 Ga metamorphic event (Xiu et al., 2002, 2004; Dan et al., 2012; Gong et al., 2011, 2012; Zhang et al., 2013a).

Geochronological data from both the Tiekelik and North Altyn–Dunhuang and Alashan regions suggest that the major tectonothermal events temporally overlap (Fig. 12). We therefore propose a Tiekelik–North Altyn–Dunhuang–Alashan connection during the Paleoproterozoic (i.e. a Tarim–North China craton connection), although there are controversies suggesting that the Alashan block was connected with the Yinshan block, the Khondalite Belt and North Hebei Orogenic Belt (Zhao et al., 2005; Geng et al., 2010; Kusky et al., 2007; Zhang et al., 2013a).

6. Conclusions

U–Pb dating of zircons from metamorphic, magmatic and sedimentary rocks from the Tiekelik Belt (southwestern Tarim craton) provides new insights into the Paleoproterozoic geological evolution of this terrane. Results from the present study are summarized as follow:

(1) Magmatic-looking zircons from orthogneisses within the Heluositan Complex (former Group) display ages of 2310 to 2260 Ma, that we interpret as the crystallization age of the granitoid protolith.
(2) The same two gneiss samples from the Heluositan Complex yielded metamorphic ages at 2040–2007 Ma and 1830 Ma, that we interpret to result from crustal reworking in the Tiekelik Belt.
(3) Geochemical and geochronological studies suggest that high-K calc–alkaline, A-type syenogranites belonging to the Buweituwei pluton were emplaced at 1900 and 1795 Ma ago. The first age is contemporaneous with 1.9 Ga mafic dykes that intrude the Heluositan Complex. We interpret that the BP peraluminous syenogranites might be produced by partial melting of ferroan granodiorite over 4 kbar.

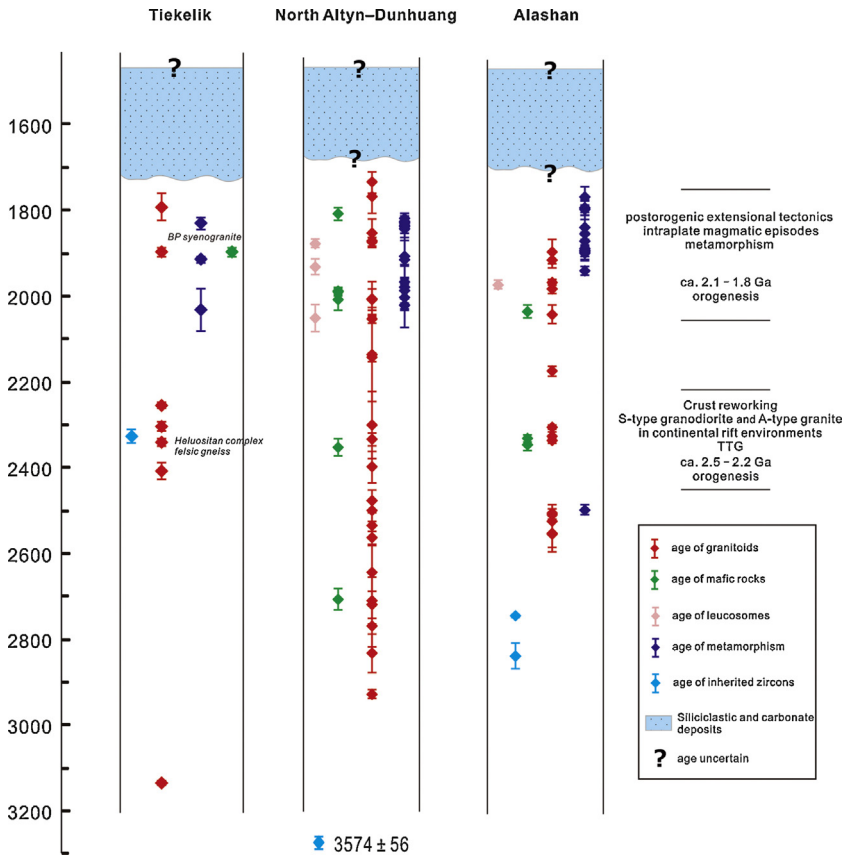

Fig. 12. Archean and Palaeoproterozoic tectonothermal events and sedimentary units in the Tiekelik Belt, North Altyn–Dunhuang and Alashan blocks. See text for details, sources and discussion.

(4) The sedimentary sequences in this study (possibly Mesoproterozoic) overlying the Paleoproterozoic granitoids. The distribution of detrital zircon grains in the sediments indicates derivation from local basement rocks. The maximum deposition ages (youngest detrital zircon grain) vary from 1.95 Ga to 1.85–1.78 Ga; however, the exact age of this sedimentary sequence is poorly constrained although we favor association with the Changcheng interval (1.8–1.6 Ga).

(5) A large number of geochronological data from the Tiekelik and North Altyn–Dunhuang and Alashan suggest that the major tectonothermal events are similar during the Paleoproterozoic. We therefore propose a Tarim Craton and North China Craton within the Columbia supercontinent at that time.

Acknowledgements

This work is supported by the National Natural Science Foundation of China (Grant No. 40902022), China Geological Survey (Grant No. 1212010610102 and One Hundred Distinguished Young Geoscientists Program), and the Science and Technology Planning Project of Shaanxi Province, China (Grant No. 2014KJXX-19). This manuscript has benefited greatly from the critical and constructive comments of Drs. Åke Johansson and Fawna Korhonen. Drs. Xiaoming Liu, Hujun Gong, and Chunrong Diwu are thanked for their technical assistance.

Appendix A. Supplementary data

Supplementary data associated with this article can be found, in the online version, at http://dx.doi.org/10.1016/j.precamres.2014.08.018.

References

Anderson, J.L., 1983. Proterozoic anorogenic granitoid plutonism of North America. In: Medaris, J., Byers, C.W., Mickelson, D.M., Shanks, W.C. (Eds.), Proterozoic Geology, Selected Papers From an International Symposium, vol. 161. Geological Society of America Memoir, pp. 133–154.

BGMG, 1989. Regional Geology of Gansu Province. Geological Publishing House, Beijing, pp. 10–12 (in Chinese).

Bogaerts, M., Scaillet, B., VanderAuwera, J., 2006. Phase equilibria of the Lyngdal granodiorite (Norway): implications for the origin of metaluminous ferroan granitoids. J. Petrol. 47, 2405–2431.

Bonin, B., 2007. A-type granites and related rocks: evolution of a concept, problems and prospects. Lithos 97, 1–29.

Che, Z.C., Sun, Y., 1996. The age of the Altun granulite facies complex and the basement of the Tarim basin. Region. Geol. China 56, 51–57 (in Chinese with English abstract).

Clemens, J.D., Holloway, J.R., White, A.J.R., 1986. Origin of A-type granites, experimental constraints. Am. Mineral. 71, 317–324.

Collins, W.J., Beams, S.D., White, A.J.R., Chappell, B.W., 1982. Nature and origin of A-type granites with particular reference to southeastern Australia. Contrib. Mineral. Petrol. 80, 189–200.

Corfu, F., Hanchar, J.M., Hoskin, P.W.O., Kinny, P., 2003. Atlas of zircon textures. Rev. Mineral. Geochem. 53, 469–500.

Creaser, R.A., Price, R.C., Wormald, R.J., 1991. A-type granites revisited: assessment of a residual-source model. Geology 19, 163–166.

Dan, W., Li, X.H., Guo, J.H., Liu, Y., Wang, X.C., 2012. Paleoproterozoic evolution of the eastern Alxa Block, westernmost North China: evidence from in situ zircon U–Pb dating and Hf–O isotopes. Gondwana Res. 12, 838–864.

Eby, G.N., 1990. The A-type granitoids: a review of their occurrence and chemical characteristics and speculations on their petrogenesis. Lithos 26, 115–134.

Frost, C.D., Frost, B.R., 1997. Reduced rapakivi-type granites: the tholeiite connection. Geology 25, 647–650.

Frost, B.R., Frost, C.D., 2008. A geochemical classification for feldspathic igneous rocks. J. Petrol. 49, 1955–1969.

Frost, C.D., Frost, B.R., 2011. On ferroan (A-type) granitoids: their compositional variability and modes of origin. J. Petrol. 52, 39–55.

Frost, B.R., Barnes, C.G., Collins, W.J., Arculus, R.J., Ellis, D.J., Frost, C.D., 2001. A geochemical classification for granitic rocks. J. Petrol. 42, 2033–2048.

Gao, Z.J., Zhu, C.S., 1984. Precambrian Geology in Xinjiang, China. Xinjiang People's Publishing House, Urumuqi, pp. 151 (in Chinese).

Ge, R.F., Zhu, W.B., Wu, H.L., He, J.W., Zheng, B.H., 2013. Zircon U–Pb ages and Lu–Hf isotopes of Paleoproterozoic metasedimentary rocks in the Korla Complex, NW China: implications for metamorphic zircon formation and geological evolution of the Tarim Craton. Precambrian Res. 231, 1–18.
Gehrels, G.E., Yin, A., Wang, X., 2003. Magmatic history of the northeastern Tibetan Plateau. J. Geophys. Res. 108, 1–14.
Geng, Y.S., Wang, X.S., Shen, Q.H., 2006. Redefinition of the Alax Group of Precambrian metamorphic basement in Alax region, Inner Mongolia. Geol. China 33, 138–145 (in Chinese with English abstract).
Geng, Y.S., Wang, X.S., Shen, Q.H., 2007. Chronology of the Precambrian metamorphic series in the Alax, Inner Mongolia. Geol. China 34, 251–261 (in Chinese with English abstract).
Geng, Y.S., Wang, X.S., Wu, C.M., 2010. Late-Paleoproterozoic tectonothermal events of the metamorphic basement in Alxa area: evidence from geochronology. Acta Petrol. Sin. 26, 1159–1170 (in Chinese with English abstract).
Gong, J.H., Zhang, J.X., Yu, S.Y., 2011. The origin of Longshoushan Group and associated rocks in the Southern part of the Alxa Block: constraint from LA-ICP-MSU–Pb zircon dating. Acta Petrol. Mineral. 30, 795–818 (in Chinese with English abstract).
Gong, J.H., Zhang, J.X., Yu, S.Y., Li, H.K., Hou, K.J., 2012. ~2.5 Ga TTG gneiss and its geological implications in the western Alxa block, North China Craton. Chin. Sci. Bull. 57, 4064–4076.
Grant, M.L., Wilde, S.A., Wu, F.Y., Yang, J.H., 2009. The application of zircon cathodoluminescence imaging, Th–U–Pb chemistry and U–Pb ages in interpreting discrete magmatic and high-grade metamorphic events in the North China Craton at the Archean/Proterozoic boundary. Chem. Geol. 261, 155–171.
Guo, Z.J., Zhang, Z.C., Liu, S.W., Li, H.M., 2003. U–Pb geochronological evidence for the early Precambrian Complex of the Tarim Craton, NW China. Acta Petrol. Sin. 19, 537–542 (in Chinese with English abstract).
Guo, X.C., Zheng, Y.Z., Gao, J., Zhu, Z.X., 2013. Determination and geological significance of the MesoArchean Craton in Western Kunlun Mountains, Xinjiang, China. Geol. Rev. 59 (3), 401–412 (in Chinese with English abstract).
Han, Q., Zhu, Y.H., Zhu, C.L., Wang, C., Chen, Z.L., Fei, J.W., 2014. Petrological characteristics and zircon U–Pb age for the magmatic rocks from the Precambrian basement of SDQ area of Shaya rise in Tarim basin, NW China. Petrol. Sin. (in Chinese with English abstract, in press).
Harris, N.B.W., Inger, S., 1992. Trace element modeling of pelite-derived granites. Contrib. Mineral. Petrol. 110, 46–56.
He, Z.Y., Zhang, Z.M., Zong, K.Q., Dong, X., 2013. Paleoproterozoic crustal evolution of the Tarim Craton: constrained by zircon U–Pb and Hf isotopes of meta-igneous rocks from Korla and Dunhuang. J. Asian Earth Sci. 78, 54–70.
HNGS, 2004. Geological Map of Yecheng County, Xinjiang, China, Scale 1:250,000. Regional Geological Survey Institute of Hunan Province (in Chinese).
Hou, G., Santosh, M., Qian, X., Lister, G.S., Li, J., 2008. Configuration of the Late Paleoproterozoic supercontinent Columbia: insights from radiating mafic dyke swarms. Gondwana Res. 14, 395–409.
Hu, A.Q., Rogers, G., 1992. Discovery of 3.3 Ga Archaen rocks in north Tarim Block of Xinjiang, western China. Chin. Sci. Bull. 37, 1546–1549.
Huang, J.G., Yang, R.D., Yang, J., Cui, C.L., Hou, L.J., 2012. Mesoproterozoic magmatic activity and its geological significance in Kusilafu area of the northern margin of western Kunlun. Chin. J. Geol. 47 (3), 867–885 (in Chinese with English abstract).
Kusky, T.M., Li, J.H., Santosh, M., 2007. The Paleoproterozoic North Hebei Orogen: North China Craton's collisional suture with the Columbia supercontinent. Gondwana Res. 12, 4–28.
Le Maitre, R.W. (Ed.), 1989. A Classification of Igneous Rocks and Glossary of Terms. Blackwell, Oxford, p. 193.
Li, H.M., Lu, S.N., Zheng, J.K., 2001. Dating of 3.6 Ga zircon in granite gneiss from the eastern Altyn Mountain and its geological significance. J. Bull. Mineral. Petrol. Geochem. 20, 259–262 (in Chinese).
Loiselle, M.C., Wones, D., 1979. Characteristics and origin of anorogenic granites. Geol. Soc. Am. Abstr. Progr. 11, 468.
Long, X.P., Yuan, C., Sun, M., Zhao, G.C., Xiao, W.J., Wang, Y.J., Yang, Y.H., Hu, A.Q., 2010. Archean crustal evolution of the Tarim Craton, NW China: zircon U–Pb and Hf isotopic constraints and implications. Precambrian Res. 180, 272–284.
Long, X.P., Sun, M., Yuan, C., Kröner, A., Hu, A.Q., 2012. Zircon REE patterns and geochemical characteristics of Paleoproterozoic anatectic granite in the northern Tarim Craton, NW China: implications for the reconstruction of the Columbia supercontinent. Precambrian Res. 222–223, 474–487.
Lu, S.N., Yuan, G.B., 2003. Geochronology of early Precambrian magmatic activity in Aketasdhtage, East Altyn tagh. Acta Geol. Sin. 77, 61–68 (in Chinese with English abstract).
Lu, S.N., Li, H.K., Zhang, C.L., Niu, G.H., 2008. Geological and geochronological evidence for the Precambrian evolution of the Tarim craton and surrounding continental fragments. Precambrian Res. 160, 94–107.
Ludwig, K.R., 2003. Isoplot 3.0: A Geochronological Toolkit for Microsoft Excel. Berkeley Geochronology Center, Special Publication, pp. 1–70.
Ma, S.P., Wang, Y.Z., Fang, X.L., 1991. Basic characteristics of Proterozoic eonothem as a table cover on northern slope of the western Kunlun Mountains. Xinjiang Geol. 9, 59–70 (in Chinese with English abstract).
Ma, X.X., Shu, L.S., Jahn, B.M., Zhu, W.B., Faure, M., 2013. Precambrian tectonic evolution of Central Tianshan, NW China: constraints from U–Pb dating and in situ Hf isotopic analysis of detrital zircons. Precambrian Res. 231, 1–18.
Meert, J.G., 2002. What's in a name? The Columbia (Palaeopangea/Nuna) supercontinent. Gondwana Res. 21, 987–993.
Meert, J.G., 2012. What's in a name? The Columbia (Palaeopangea/Nuna) supercontinent. Gondwana Res. 21, 987–993.
Meert, J.G., 2014. Strange attractors, spiritual interlopers and lonely wanderers: the Search for Pre-Pangæan supercontinents. Geosci. Front. 5, 155–166.
Möller, A., Hensen, B.J., Armstrong, R.A., Mezger, K., Ballèvre, M., 2003. U–Pb zircon and monazite age constraints on granulite-facies metamorphism and deformation in the Strangways Metamorphic Complex. Contrib. Mineral. Petrol. 145, 406–423.
Patiño Douce, A.E., 1997. Generation of metaluminous A-type granites by low-pressure melting of calc–alkaline granitoids. Geology 25, 743–746.
Patiño Douce, A.E., 1999. What do experiments tell us about the relative contributions of crust and mantle to the origin of granitic magmas? In: Castro, A., Fernandez, C., Vigneresse, J.L. (Eds.), Understanding Granites: Integrating New and Classical Techniques, 168. Geological Society of London Special Publications, pp. 55–75.
Peng, C.W., Gao, Z.J., 1988. Microflora and stromatolites from the late Precambrian on the northern slope of west Kunlun mountains and their stratigraphic significance. Xinjiang Geol. 2, 17–28 (in Chinese with English abstract).
Ren, J.S., Jiang, C.F., Zhang, Z.K., 1980. Tectonics and Evolution of China. Science Press, Beijing, pp. 1–124 (In Chinese).
RGXR, 1993. Regional geology of Xinjiang Uygur Autonomous Region. Geological Publishing House, Beijing, pp. 1–841 (in Chinese).
Rickwood, P.C., 1989. Boundary lines within petrologic diagrams which use oxides of major and minor elements. Lithos 22, 247–263.
Rogers, J.J.W., Santosh, M., 2002. Configuration of Columbia, a Mesoproterozoic supercontinent. Gondwana Res. 5, 5–22.
Rogers, J.J.W., Santosh, M., 2009. Tectonics and surface effects of the supercontinent Columbia. Gondwana Res. 15, 373–380.
Shu, L.S., Deng, X.L., Zhu, W.B., Ma, D.S., Xiao, W.J., 2011. Precambrian tectonic evolution of the Tarim Block, NW China: new geochronological insights from the Quruqtagh domain. J. Asian Earth Sci. 42, 774–790.
Sircombe, K.N., 2004. AgeDisplay: an Excel workbook to evaluate and display univariate geochronological data using binned frequency histograms and probability density distributions. Comput. Geosci. 30, 21–31.
Skjerlie, K.P., Johnston, A.D., 1992. Vapor-absent melting at 10 kbar of a biotite and amphibole bearing tonalitic gneiss, implications for the generation of A-type granites. Geology 20, 263–266.
Skjerlie, K.P., Johnston, A.D., 1993. Fluid-absent melting behaviour of an F-rich tonalitic gneiss at mid-crustal pressures: implications for the generation of anorogenic granites. J. Petrol. 34, 785–815.
Streckeisen, A., Le Maitre, R.W., 1979. A chemical approximation to the modal QAPF classification of igneous rocks. Neues Jahrbuch für Mineralogie (Abhandlungen) 136, 169–206.
Sun, S.S., McDonough, W.F., 1989. Chemical and isotopic systematics of oceanic basalts; implications for mantle composition and processes. In: Saunders, A.D., Norry, M.J. (Eds.), Magmatism in the Ocean Basins, 42. Geological Society of London Special Publications, pp. 313–345.
Tung, G.A., Yang, H.Y., Liu, D.Y., Zhang, J.X., Tseng, C.Y., Wan, Y.S., 2007. SHRIMPU–Pb geochronology of the detrital zircons from the Longshoushan Group and its tectonic significance SHRIMP U–Pb geochronology of the detrital zircons from the Longshoushan Group and its tectonic significance. Chin. Sci. Bull. 52, 1414–1425.
Turner, S.P., Foden, J.D., Morrison, R.S., 1992. Derivation of some A-type magmas by fractionation of basaltic magma; an example from the Padthaway Ridge, South Australia. Lithos 28, 151–179.
Wang, C., (Ph.D. thesis) 2011. Precambrian Tectonics of the Southern Margin of Tarim Basin, NW China. Northwest University, China (in Chinese with English abstract).
Wang, A.G., Zhang, C.L., Zhao, Y., Guo, K.Y., Dong, Y.G., 2004. Depositional types of the lower part of Nanhua System on the northern margin of southwest Tarim and tectonic significance. J. Stratigr. 28, 248–256 (in Chinese with English abstract).
Wang, C., Liu, L., Li, R.S., He, S.P., Yang, W.Q., Cao, Y.T., Zhu, X.H., 2009. U–Pb isotopic ages and Hf isotopic composition of single zircons from Heluositan Group: implications for Paleoproterozoic juvenile continental crust and reworking at the southwestern margin of Tarim Carton. In: National Symposium on Petrology and Geodynamics Abstracts 2009. Jilin University (in Chinese).
Wang, C., Liu, L., Xiao, P.X., Cao, Y.T., Yu, H.Y., Meert, J., Liang, W.T., 2014. Geochemical and geochronologic constraints for Paleozoic magmatism related to the orogenic collapse in the Qimantagh–South Altyn region, northwestern China. Lithos 202/203, 1–20.
Wang, C., Liu, L., Wang, Y.H., Li, R.S., He, S.P., Li, M., Collins, A., Yang, W.Q., Cao, Y.T., Shi, C., Yu, H.Y., 2014. Recognition and tectonic implications of an extensive Neoproterozoic volcano-sedimentary rift basin along the southwestern margin of the Tarim Craton, northwestern China. Precambrian Res. (submitted for publication).
Whalen, J.B., Currie, K.L., Chappell, B.W., 1987. A-type granites: geochemical characteristics, discrimination and petrogenesis. Contrib. Mineral. Petrol. 95, 407–419.
Wright, J.B., 1969. A simple alkalinity ratio and its application to question of non-orogenic granite gneisses. Geol. Mag. 106, 370–384.
Wu, J.S., Geng, Y.S., Shen, Q.H., Wan, Y.S., Liu, D.Y., Song, B., 1998. Archean Geology Characteristics and Tectonic Evolution of Sino-Korea Paleocontinent. Geological Publishing House, Beijing, pp. 1–212 (in Chinese).
Wu, G.H., Li, H.W., Xu, Y.L., Su, W., Chen, Z.Y., Zhang, B.S., 2012. The tectonothermal events, architecture and evolution of Tarim craton basement palaeo-uplifts. Acta Petrol. Sin. 28 (8), 2435–2452 (in Chinese with English abstract).
Xin, H.T., Zhao, F.Q., Luo, Z.H., Liu, Y.S., Wan, Y.S., Wang, S.Q., 2011. Determination of the Paleoproterozoic geochronological framework in Aqtashtagh area

in Southeastern Tarim, China, and its geological significance. Acta Geol. Sin. 85, 1977–1993 (in Chinese with English abstract).
Xin, H.T., Liu, Y.S., Luo, Z.H., Song, S.C., Wang, S.Q., 2013. The growth of Archean continental crust in Aqtashtagh area of southeast Tarim, China: constraints from petrochemistry and chronology about Milan Group and TTG gneiss. Earth Sci. Front. 20, 240–259 (in Chinese with English abstract).
Xiu, Q.Y., Lu, S.N., Yu, H.F., 2002. The isotopic age evidence for main Longshoushan group contributing to Palaeoproterozoic. Prog. Precambrian Res. 25, 93–96 (In Chinese with English abstract).
Xiu, Q.Y., Yu, H.F., Li, Q., 2004. Discussion on the petrogenic time of Longshoushan Group, Gansu Province. Acta Geol. Sin. 78, 366–373 (in Chinese with English Abstract).
Xu, R.H., Zhang, Y., 1996. Isotopic geochemistry of plutonic rocks. In: Pan, Y. (Ed.), Geological Evolution of the Karakorum and Kunlun Mountains. Seismological Press, Beijing, pp. 138–186.
Xu, Z.Q., He, B.Z., Zhang, C.L., Zhang, J.X., Wang, Z.M., Cai, Z.H., 2013. Tectonic framework and crustal evolution of the Precambrian basement of the Tarim Block in NW China: new geochronological evidence from deep drilling samples. Precambrian Res. 235, 150–162.
Yakubchuk, A., 2010. Restoring the supercontinent Columbia and tracing its fragments after its breakup: a new configuration and a Super-Horde hypothesis. J. Geodyn. 50, 166–175.
Yang, J.Q., Wan, Y.S., Liu, Y.S., Xin, H.T., Zhang, S.R., Li, M.E., 2012. Discovery of Paleoproterozoic crustal derived carbonatite in the Northern Altyn Tagh. Earth Sci. J. China Univ. Geosci. 37, 929–936 (in Chinese with English abstract).
Yuan, H.L., Gao, S., Liu, X.M., Li, H.M., Günther, D., Wu, F.Y., 2004. Accurate U–Pb age and trace element determinations of zircon by laser ablation inductively coupled plasma-mass spectrometry. Geostand. Geoanal. Res. 11, 357–370.
Zhai, M.G., Bian, A.G., 2000. The amalgamation of the supercontinent of North China Craton at the end of Neoarchean and its breakup during late Paleoproterozoic and Mesoproterozoic sup. Sci. China D 30, 129–137.
Zhai, M.G., Santosh, M., 2011. The early Precambrian odyssey of North China Craton: a synoptic overview. Gondwana Res. 20, 6–25.
Zhang, C.L., Ye, H.M., Wang, A.G., Guo, K.Y., Dong, Y.G., 2004. Geochemistry of the Neoproterozoic diabase and basalt in the south of Tarim plate: evidence for the Neoproterzoic breakup of the Rodinia supercontinent in the south of Tarim. Acta Petrol. Sin. 20, 473–482 (in Chinese with English abstract).
Zhang, C.L., Li, X.H., Li, Z.X., Lu, S.N., Ye, H.M., Li, H.M., 2007. Neoproterozoic ultramafic–mafic–carbonatite Complex and granitoids in Quruqtagh of northeastern Tarim block, western China: geochronology, geochemistry, and tectonic implication. Precambrian Res. 152, 149–169.
Zhang, S., Li, Z.-X., Evans, D.A.D., Wu, H., Li, H., Dong, J., 2012a. Pre-Rodinia supercontinent Nuna shaping up: a global synthesis with new paleomagnetic results from North China. Earth Planet. Sci. Lett. 353/354, 145–155.
Zhang, C.L., Zou, H.B., Li, H.K., Wang, H.Y., 2012b. Tectonic framework and evolution of the Tarim Block in NW China. Gondwana Res. 23, 1306–1315.
Zhang, J.X., Gong, J.H., Yu, S.Y., 2012c. 1.85 Ga HP granulite-facies metamorphism in the Dunhuang block of the Tarim Craton, NW China: evidence from U–Pb zircon dating of mafic granulites. J. Geol. Soc. 169, 511–514.
Zhang, C.L., Li, H., Santosh, M., Li, Z., Zou, H., Wang, H., Ye, H., 2012d. Precambrian evolution and cratonization of the Tarim Block, NW China: petrology, geochemistry, Nd-isotopes and U–Pb zircon geochronology from Archean gabbro-TTG-potassic granite suite and Paleoproterozoic metamorphic Belt. J. Asian Earth Sci. 47, 5–20.
Zhang, J.X., Gong, J.H., Yu, S.Y., Li, H.K., Hou, K.J., 2013a. Neoarchean–Paleoproterozoic multiple tectonothermal events in the western Alxa block, North China Craton and their geological implication: evidence from zircon U–Pb ages and Hf isotopic composition. Precambrian Res. 235, 36–57.
Zhang, J.X., Yu, S.Y., Gong, J.H., Li, H.K., Hou, K.J., 2013b. The latest NeoArchean–Paleoproterozoic evolution of the Dunhuang block, eastern Tarim craton, northwestern China: evidence from zircon U–Pb dating and Hf isotopic analyses. Precambrian Res. 226, 21–42.
Zhao, G.C., Cawood, P.A., 2012. Precambrian geology of China. Precambrian Res. 222/223, 13–54.
Zhao, G.C., Zhai, M.G., 2012. Lithotectonic elements of Precambrian basement in the North China Craton: review and tectonic implications. Gondwana Res. 23, 1207–1240.
Zhao, G.C., Cawood, P.A., Wilde, S.A., Sun, M., 2002. Review of global 2.1–1.8 Ga orogens: implications for a pre-Rodinia supercontinent. Earth Sci. Rev. 59, 125–162.
Zhao, G.C., Sun, M., Wilde, S.A., Li, S.Z., 2004. A Paleo-Mesoproterozoic supercontinent: assembly, growth and breakup. Earth Sci. Rev. 67, 91–123.
Zhao, G.C., Sun, M., Wilde, S.A., Li, S.Z., 2005. Late Archean to Paleoproterozoic evolution of the North China Craton: key issues revisited. Precambrian Res. 136, 177–202.
Zhao, Y., Diwu, C.R., Sun, Y., Zhu, T., Wang, H.L., 2013. Zircon geochronology and Lu–Hf isotope compositions for Precambrian rocks of the Dunhuang Complex in Shuixiakou area, Gansu Province. Acta Petrol. Sin. 29, 1698–1712 (in Chinese with English abstract).
Zong, K., Liu, Y., Zhang, Z., He, Z., Hu, Z., Guo, J., Chen, K., 2013. The generation and evolution of Archean continental crust in the Dunhuang block, northeastern Tarim craton, northwestern China. Precambrian Res. 235, 251–263.